universe

MDPI

*Review*

# Probing Supernova Diversity Through High-Cadence Optical Observations

**Kuntal Misra [1,*], Bhavya Ailawadhi [1], Raya Dastidar [2], Monalisa Dubey [1,3], Naveen Dukiya [1,3], Anjasha Gangopadhyay [4], Divyanshu Janghel [1,3], Kumar Pranshu [1,5] and Mridweeka Singh [6]**

1 Aryabhatta Research Institute of Observational Sciences (ARIES), Manora Peak, Nainitl 263001, India; monalisa@aries.res.in (M.D.)
2 Millennium Institute of Astrophysics, Nuncio Monseñor Sótero Sanz 100, Santiago 8320000, Chile
3 Department of Applied Physics, Mahatma Jyotiba Phule Rohilkhand University, Bareilly 243006, India
4 Department of Astronomy, Oskar Klein Center, Stockholm University, SE-106 91 Stockholm, Sweden
5 Department of Applied Optics and Photonics, University of Calcutta, Kolkata 700106, India
6 Indian Institute of Astrophysics, Koramangala 2nd Block, Bangalore 560034, India
* Correspondence: kuntal@aries.res.in

## Abstract

Supernovae (SNe) are among the most energetic and transient events in the universe, offering crucial insights into stellar evolution, nucleosynthesis, and cosmic expansion. Optical observations have historically played a central role in the discovery, classification, and physical interpretation of SNe. In this review, we summarize recent progress in the optical study of SNe, with a focus on advancements in time-domain surveys and photometric and spectroscopic follow-up strategies. High-cadence optical monitoring is pivotal in capturing the diverse behaviors of SNe, from early-time emission to late-phase decline. Leveraging data from ARIES telescopes and national/international collaborations, we systematically investigate various SN types, including Type Iax, IIP/L, IIb, IIn/Ibn and Ib/c events. Our analysis includes light curve evolution and spectral diagnostics, providing insights into early emission signatures (e.g., shock breakout), progenitor systems, explosion mechanisms, and circumstellar medium (CSM) interactions. Through detailed case studies, we demonstrate the importance of both early-time and nebular-phase observations in constraining progenitor and CSM properties. This comprehensive approach underscores the importance of coordinated global efforts in time-domain astronomy to deepen our understanding of SN diversity. We conclude by discussing the challenges and opportunities for future optical studies in the era of wide-field observatories such as the Vera C. Rubin Observatory (hereafter Rubin), with an emphasis on detection strategies, automation, and rapid-response capabilities.

**Keywords:** supernova; thermonuclear supernovae; core collapse supernovae; optical observations; photometry; spectroscopy



Academic Editors: Vikram Dwarkadas and Lorenzo Iorio

Received: 26 August 2025
Revised: 10 October 2025
Accepted: 17 October 2025
Published: 31 October 2025

**Citation:** Misra, K.; Ailawadhi, B.; Dastidar, R.; Dubey, M.; Dukiya, N.; Gangopadhyay, A.; Janghel, D.; Pranshu, K.; Singh, M. Probing Supernova Diversity Through High-Cadence Optical Observations. *Universe* **2025**, *11*, 361. https://doi.org/10.3390/universe11110361



## 1. Introduction

Supernovae (SNe) are energetic explosions that mark the final stages of stellar evolution. They can either arise from the core-collapse of a massive star (Core-Collapse SN or CCSN) or a thermonuclear explosion of white dwarfs. The study of SNe carries vast implications in many aspects of astrophysics. While lighter elements are synthesized in stellar cores prior to the explosion, SNe are primarily responsible for the formation and distribution of elements heavier than iron. These elements are the building blocks of

planet formation and the biochemistry of life itself. They are the progenitors of all compact objects like neutron stars and black holes. SN influence galactic evolution and dynamics by disrupting interstellar gas and dust clouds, triggering star formation. Type Ia SNe are used as "standard candles" and provide an important rung in the current cosmic distance ladder to measure cosmological distances. Additionally, it has been theorized that SNe can contribute significantly to the cosmic rays and the cosmic dust budget.

From the diverse physical conditions that can result from the complexities of stellar evolution, SNe show a great diversity among themselves. They are traditionally classified based on their early-time (peak) spectra, which provide the most immediate and accessible diagnostic information [1]. The primary distinction is between Type I SNe, which lack hydrogen lines in their spectra, and Type II SNe, which exhibit prominent hydrogen features [2]. These types are further subdivided into several subtypes based on the presence/absence of other elements (such as helium and silicon) and the evolution of their light curves and spectra over time. Among the various subtypes, only Type Ia originates from thermonuclear explosions of white dwarfs in binary systems and is identified by the presence of strong Si II absorption features in its spectra. Contrary to Type Ia SNe, all other SNe are considered to result from the gravitational collapse of massive stars $\gtrsim$8 $M_\odot$ [3].

The Type II SNe are further divided into IIP, IIL, IIb, and IIn. Traditionally, the classification between Type IIP and IIL is based on the light curve decline rate from the peak luminosity; however, recent studies have shown that the IIP/IIL/IIb subtypes can be explained as part of a continuous population with decreasing hydrogen envelope mass before the SN explosion [4–6]. The hydrogen-deficient SNe are classified as Type Ib (presence of He) and Ic (lack of He). This classification scheme, despite being empirically motivated, subtly reveals the mass-loss hierarchy in stellar evolution. This classification paradigm and the prominent classes are shown in Figure 1.

The observed variety among CCSNe has been traditionally attributed mainly to differences in the progenitor star's initial mass, composition, rotation, and explosion energy. However, the Circumstellar Material (CSM) plays an equally critical role in shaping the explosion outcomes. Massive stars undergo substantial mass loss during their lifetimes through stellar winds, binary interactions, and eruptive outbursts [7]. This expelled material accumulates around the star as CSM. The CSM around the progenitor star can become ionized from the shock-breakout emission or continued shock interaction with the CSM itself. When the CSM recombines, narrow lines are seen in the spectra, characteristic of the slow CSM velocity. Depending on the extent and density of the CSM, its effect can manifest anywhere from short-lived flash-ionization features seen early in the spectrum of SNe [8,9] to interaction features seen in SNe lasting years, even decades [10,11]. Since mass loss is such a ubiquitous phenomenon, CSM is ever-present in the surroundings of massive stars, albeit with different densities and configurations. However, electromagnetic emissions from interaction with low-density CSM can be too faint to be detected. But many SNe can have dense CSM in the immediate vicinity of the progenitor star, giving rise to flash features [8]. On the contrary, SNe can also have dense CSM that is located at a distance that eventually shows interaction signatures, as the high-energy photons from the shock breakout or the SN ejecta itself reach distant CSM [12–15]. SNe that show lasting interaction with dense CSM through most of their lifetime are called interacting SNe. They show narrow spectral lines and are distinguished with the letter 'n' in the usual SN taxonomy. SNe of Type IIn are distinguished by the presence of narrow H lines in the spectra. Similarly, Type Ibn and Icn SNe show narrow lines of He and C/N/O, respectively. The presence of CSM can complicate the studies of SNe, but in turn, it provides valuable insights into the pre-explosion mass-loss processes and the final phases of stellar evolution.

In this review article, we discuss various aspects of the optical emission from SNe. The light curves and spectra of the different subtypes of SNe are presented and compared at different phases of SN evolution. The explosion and progenitor properties of SNe, such as the initial mass of the progenitor, pre-SN mass and radius, explosion asymmetry, etc., derived from the optical observations are also discussed in this review. We have taken representative SNe of different subtypes, which were studied by our group. However, this may not represent the entire diverse population and progenitors of SNe.

A valuable resource for researchers on SNe is the book on "Supernova Explosions" by David Branch and Craig J. Wheeler [16], which provides a comprehensive introduction to SNe, including the historical development of the field, their observational characteristics, combined with theoretical models.

The paper is structured as follows: the detection and observations of SNe are discussed in Section 2. The properties of rare Type Iax SNe are discussed in Section 3. A detailed discussion on CCSNe of Type IIP/L is presented in Section 4, followed by the stripped envelope SNe in Section 5. The properties of the interacting class of SNe are elaborated in Section 6. A summary based on this study is given in Section 7.

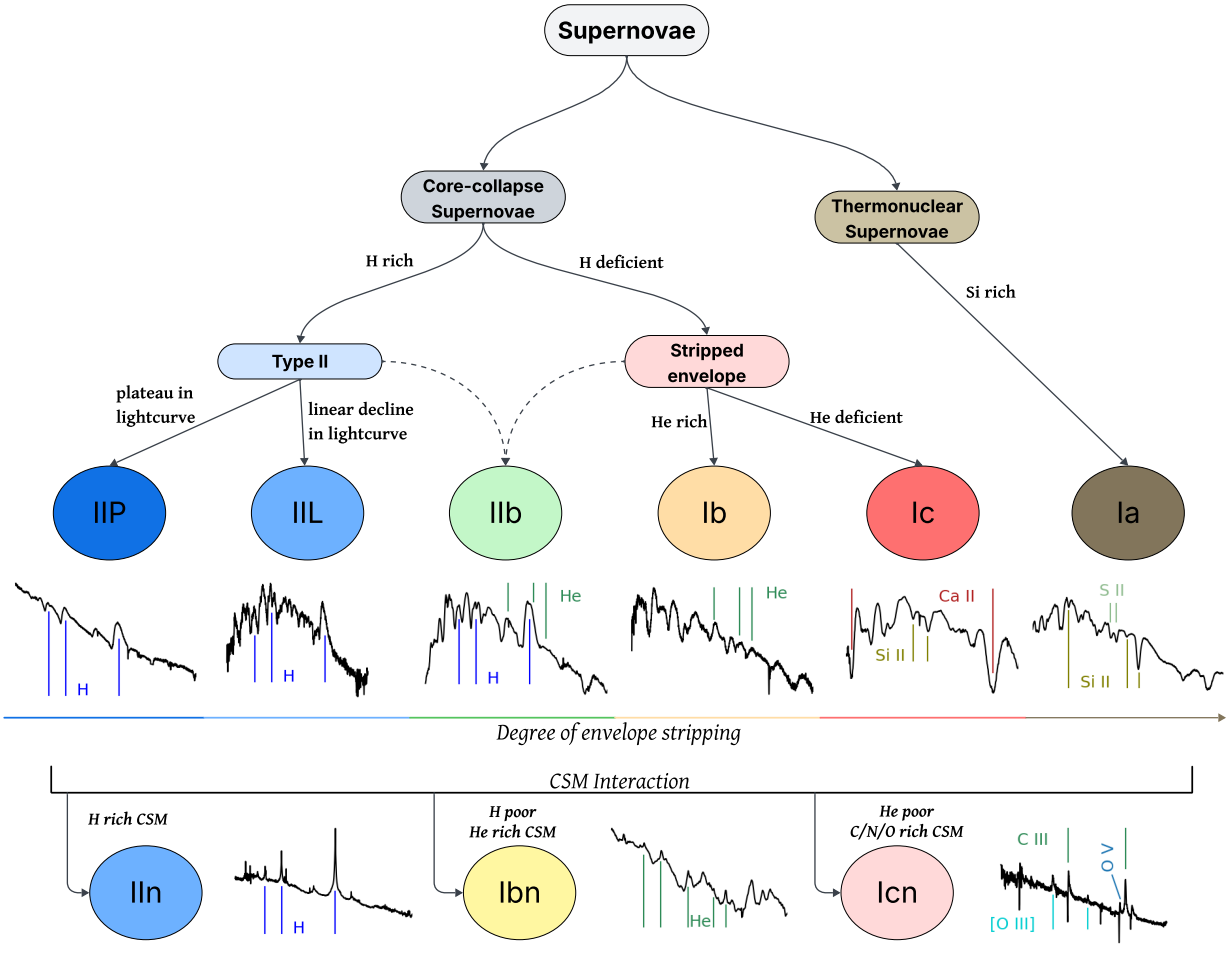


**Figure 1.** The traditional classification scheme of SNe. The envelope stripping increases as we go from left to right in the figure. The bottom panel shows the interacting SNe where the spectrum is primarily influenced by CSM constitution, especially at early phases. Each subtype is shown with a representative spectra near peak light (SNe 1999em [17], 2014G [18], 1993J [19], 2007Y [20], 1994I [21], 2011fe [22], 2010jl [23], 2006jc [24], 2019hgp [25]).

## 2. Detection and Observation of SNe

SNe are a rare class of extragalactic transients that are often discovered with the help of dedicated transient survey programs. These can be in the form of a sky transient survey, where the imaging is performed over the entire visible sky area. Depending on the science requirement, the imaging is scheduled at a predefined cadence. Modern surveys usually employ automated techniques for transient search in the large volumes of acquired image data. Examples include the Zwicky Transient Facility (ZTF, [26]), Asteroid Terrestrial-impact Last Alert System ATLAS [27], Panoramic Survey Telescope and Rapid Response System Pan-STARRS [28], All Sky Automated Survey for SuperNovae ASAS-SN [29], and the new Rubin Observatory. The International Liquid Mirror Telescope ILMT [30] at the Aryabhatta Research Institute of Observational Sciences (ARIES) is India's first optical survey telescope that also uses this approach to search for transients in the visible zenith sky.

Alternatively, some transient search programs also perform a targeted survey of a predefined sample of nearby galaxies to search for transients. Such a program is often advantageous in terms of a smaller response time, enabling early detection of bright events. An example of such a program is the Distance Less than 40 Mpc survey DLT40 [31]. Additionally, amateur astronomers contribute immensely towards the early detection and reporting of bright SNe events. All detected SNe are reported by the different groups to the Transient Name Server (TNS)[1], which is the official International Astronomical Union (IAU) mechanism for reporting new astronomical transients.

### *2.1. Observing Facilities and Follow-Up Strategy*

ARIES, located in Nainital, India, operates modern optical observational facilities, including the 1.04 m Sampurnanand Telescope ST [32], 1.3 m Devasthal Fast Optical Telescope (DFOT) [33], 3.6 m Devasthal Optical Telescope (DOT) [34], and the 4 m ILMT. These telescopes are located in the Manora Peak and Devasthal Observatories of ARIES, Nainital (India)[2]. These facilities provide regular imaging and spectroscopic capabilities that are well-suited for monitoring transient astrophysical events. Their strategic location, in the middle of the wide longitude band of Eastern Australia and the Canary Islands, and dedicated follow-up programs make ARIES an important contributor to time-domain astronomy, particularly in the study of SNe, variable stars, and other rapidly evolving transients.

SN research at ARIES has utilized the data from three telescopes, *viz.* ST, DFOT and DOT. During the early bright phase of the SN, high-cadence photometric follow-up is performed using the two 1 m class telescopes (ST and DFOT) in Bessel and Sloan Digital Sky Survey (SDSS) filters. Deep photometry is performed for nebular phases with the DOT equipped with the IMAGER [35] and the ARIES Devasthal Faint Object Spectrograph and Camera ADFOSC [36]. ADFOSC is also used for spectroscopic observations of SNe brighter than 18.5 mag in the $V$-band. A complete list of the telescopes in ARIES and the backend instruments used for SNe observations is provided in Table A1.

In addition to the telescopes in ARIES, nebular phase imaging and spectroscopic observations are also acquired with the Himalayan Faint Object Spectrograph and Camera (HFOSC) instrument on the 2.01 m Himalayan Chandra Telescope (HCT) [37] located in Hanle, Ladakh (India). Our observations are further strengthened by several coordinated international campaigns, which aim to systematically fill in the existing data gaps through multi-wavelength monitoring and collaborative follow-up efforts across different observatories worldwide. One of the primary observing nodes is the Las Cumbres Observatory (LCO) [38] network of telescopes as a part of the Global Supernova Project (GSP).

With the commissioning of the 4 m ILMT, the SN research at ARIES has expanded to include the study of direct discoveries. The ILMT performs continuous monitoring

of the zenith sky with a one-day cadence, searching for new transient candidates. The telescope has a dedicated pipeline [39] that performs image subtraction in near real-time on the images acquired and produces a list of transient candidates. The candidates are then passed on to a trained convolutional neural network (CNN)-based algorithm to filter out spurious candidates. The candidates are further sub-classified into various subtypes, *viz.* variable-star-like, SN-like, and orphan (e.g., asteroid) candidates. The candidates are further cross-matched with the public catalogs to remove the known sources of variability. The good candidates with multiple detections are reported to the TNS and are monitored with the ILMT and other facilities.

### *2.2. Selection of Targets for Follow-Up Observations*

Bright SNe (discovery magnitude $< 18$) are selected for follow-up from the TNS, focusing on nearby events ($z < 0.1$) to facilitate detailed observations at different phases of the SN evolution. The declination range ($-30^\circ < \delta < +90^\circ$) is set by the observatory's latitude, covering a range of right ascension (RA) values governed by the source visibility during observing cycles. Brighter events suitable for long-term monitoring are preferred, with observations typically conducted during dark or gray nights. Data obtained from the ARIES telescopes are supplemented with data from other facilities (e.g., LCO) to improve temporal coverage and constrain the evolution across all phases. In addition, bright transients (with discovery magnitude between 15 and 19 mag in the *r*-band) discovered or identified by the ILMT are systematically followed up with the ARIES telescopes. Since the first light of the ILMT in April 2022 and by the conclusion of the last observation cycle in May 2025, 21 SN candidates have been identified with the ILMT. These include the five new discoveries *viz.* AT 2023yjc, 2024fxn, 2024zsm, 2024agkc, and 2024aifv, which were subsequently reported to the TNS.

Over the last decade (2014–2025), we have undertaken observational campaigns focused on the photometric and spectroscopic monitoring of SNe of various types. We were successful in initiating observations of nearly 160 SNe with ARIES facilities. The pie chart in Figure 2 (top) shows the distribution of SNe types in our observing sample. In the chart, Type II includes IIP, IIL, IIb, and IIn SNe. Type Ia consists of both normal Type Ia and Ia-pec SNe (91T-like, 91bg-like, Ia-CSM, and Iax). Type Ib, Ic, and Broad Lined Ic are included collectively in Type Ib/c, while Others include all other SN-like transients (e.g., Super Luminous SNe (SLSNe), Luminous Blue Variables (LBVs), Luminous Red Novae (LRNe), etc.). For some of the SNe, the observing efforts were supported by a wide range of national and international facilities, which enabled well-sampled temporal and spectral coverage. However, for some events, the observations were limited due to factors such as poor weather, faster decline of the transient, visibility, etc. The distribution of discovery magnitudes (collected from the TNS reports) of SNe subsequently observed with the ARIES facilities is shown in Figure 2 (bottom). It highlights that ARIES has successfully initiated monitoring campaigns for events spanning a wide brightness range, from 13 mag down to 21 mag. Through our monitoring campaigns, we have comprehensively studied diverse SN subtypes, and the resulting datasets have been published in numerous peer-reviewed journals.

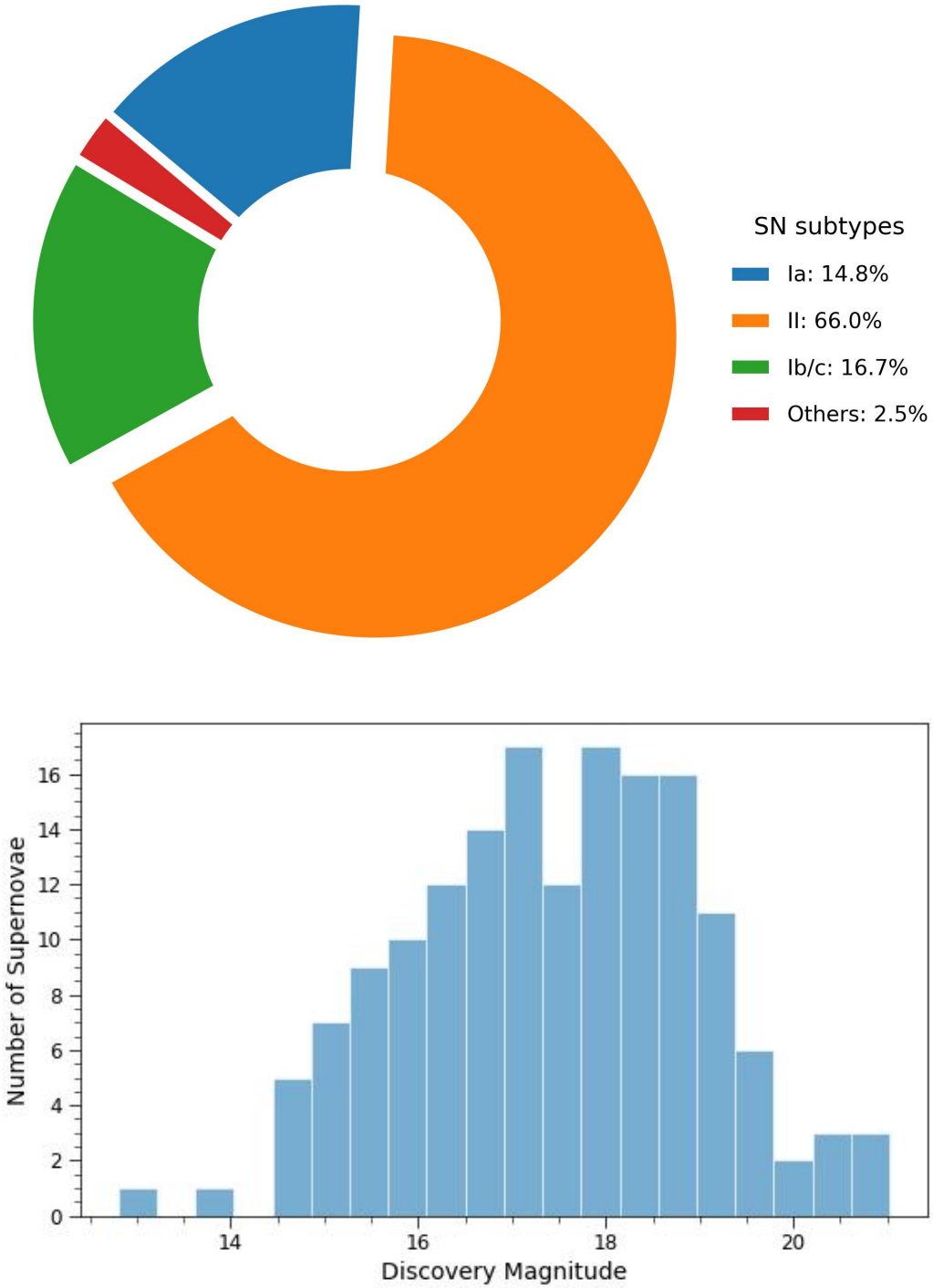


**Figure 2.** (**Top figure**): Pie chart showing the distribution of SN subtypes observed with the ARIES facilities. (**Bottom figure**): Histogram of discovery magnitudes of SNe observed with the ARIES facilities. The discovery magnitude of the SNe is collected from the TNS reports.

## 3. Tracing the Rare Type Iax Themonuclear Explosions

Type Ia SNe are believed to be the thermonuclear explosions of white dwarfs in binary systems and are identified by the presence of strong Si II absorption features in their spectra. These events are typically luminous, with a characteristic peak *B*-band absolute magnitude of about $M_B = -19.3$ mag [40]. Type Ia SNe display a well-established correlation between their peak luminosity and the subsequent decline rate of their light curves. This

empirical relation, often referred to as the Phillips relation, enables their calibration as standardizable candles, thereby making Type Ia SNe one of the most powerful tools for measuring extragalactic distances and constraining cosmological parameters [41,42]. Several peculiar subtypes of Type Ia SNe have been identified, spanning a wide luminosity range and occupying the two extremes of the distribution, with 1991T-like events [43] towards the bright end and 1991bg-like events [44] situated at the fainter end. Over the past two decades, a distinct subclass of Type Ia SNe—collectively referred to as Type Iax SNe—has emerged [45]. Type Iax SNe serve as a bridge between 1991T-like and 1991bg-like events, exhibiting luminosities comparable to 1991bg-like SNe while showing spectral features more consistent with 1991T-like SNe [45,46]. These events are estimated to occur at a rate of approximately $31^{+19}_{-13}$ for every 100 normal Type Ia SNe. Type Iax SNe differ notably from their normal counterparts in both photometric and spectroscopic characteristics. One key difference is the absence of the secondary peak typically seen in the near-infrared (NIR) light curves of normal Type Ia SNe, which is not present in Type Iax SNe [47].

### *3.1. Light Curve and Spectral Characteristics of Type Iax SNe*

Type Iax SNe are low-luminosity, peculiar cousins of Type Ia SNe. They are characterized by a wide luminosity range from $M_r = -12.7$ mag [48] to $M_B = -18.3$ mag [49]. Unlike normal Type Ia SNe, Type Iax SNe lack a secondary maximum in their NIR light curves [47]. These events typically exhibit a faster rise to maximum brightness and a more rapid decline in the bluer bands [46,50–52]. These events display a broad range in peak luminosities, corresponding to a wide spread in the synthesized $^{56}$Ni mass (varying from $8^{+4}_{-5}\times10^{-4}$ $M_\odot$ [48] to 0.3 $M_\odot$ [49]).

Spectroscopically, they exhibit weaker Si II features than normal Type Ia SNe [53], with early-time spectra dominated by Fe II, Fe III, and intermediate-mass element (IME) features, such as Ca, Mg, and Si, during early phases. Their expansion velocities are typically about half of those of normal Type Ia SNe, ranging from approximately 2000 km s$^{-1}$ [54] to 8000 km s$^{-1}$ [49,55]. At late times, their spectral evolution deviates significantly from normal Type Ia SNe. Type Iax SNe attain only a partial nebular phase; notably, a fully nebular spectrum is yet to be observed, as P-Cygni profiles remain prominent even after hundreds of days since the explosion [56]. Their late-time spectra exhibit a mix of permitted iron features along with forbidden emission lines [57].

With our first detailed analysis of a Type Iax SN 2014dt, we concluded it to be a bright Type Iax with peak absolute magnitude $M_V = -18.33 \pm 0.02$ mag [58] similar to SNe 2005hk and 2012Z. The spectroscopic features and lower photospheric velocities confirm the Type Iax nature of SN 2014dt. Interestingly, no source at the location of the SN was identified in deep pre-explosion Hubble Space Telescope (*HST*) images [59]. Different progenitor scenarios were presented for SN 2014dt, for e.g., a carbon-oxygen white dwarf with a helium-star companion [59]. Late-time Infrared (IR) excess suggests either a pre-existing dust shell from a giant companion [60] or, more plausibly, emission from a bound remnant with a super-Eddington wind [57], consistent with late-time behavior seen in Type Iax SNe.

### *3.2. Are Type Iax SNe Heterogeneous in Nature?*

Unlike Type Ia SNe, Type Iax SNe show negligible to no clear correlation between their peak luminosity and decline rates [45,50,61,62] indicating substantial heterogeneity. A few notable outliers include SNe 2007qd [61], 2009ku [62], and 2014ck [63]. Ref. [64] recently revised the earlier scaling relations using well-observed Type Iax SNe to date and proposed a possible bimodal distribution within the class (Figure 3). In the brighter subset of Type Iax SNe ($Mr \leq -17.1$ mag), there is a moderate inverse relationship between peak brightness and decline rate, with a Pearson correlation coefficient of 0.49 ($p = 0.044$),

implying that more rapidly fading SNe tend to be less luminous. Conversely, within the fainter group (M$r \geq -14.64$ mag), a strong positive trend is observed (Pearson coefficient $-0.85$, $p = 0.070$), where faster-declining SNe appear to be brighter. Given the limited number of Type Iax SNe studied to date, a larger sample encompassing the full luminosity range is necessary to verify the existence of these distinct trends. A similar study was also performed to study the correlation between peak luminosity and rise time of Type Iax SNe [50,64]. There appears to be a moderate negative correlation between brightness and rise time (Pearson coefficient = $-0.53$, $p = 0.02$), suggesting that more luminous Type Iax SNe tend to rise more slowly to peak.

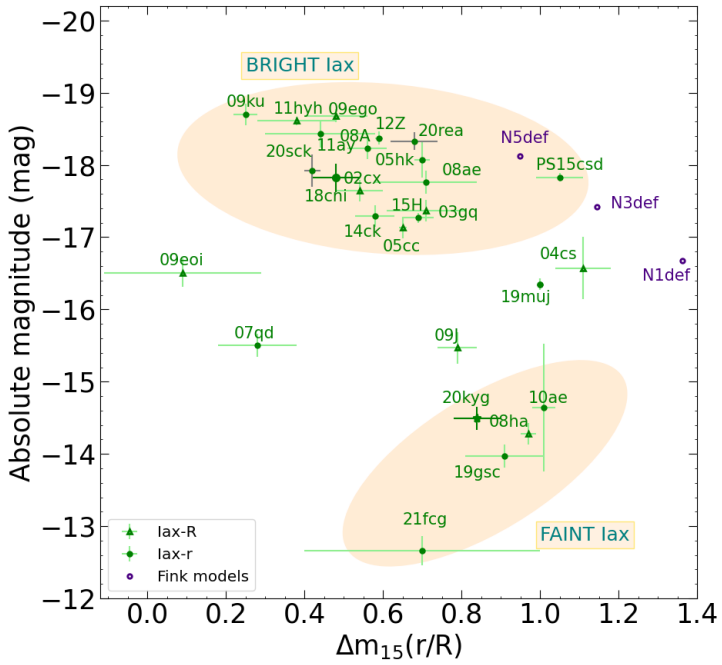


**Figure 3.** The bimodal distribution of Type Iax SNe in terms of the peak absolute magnitude and rise time in r/R-band [64].

### *3.3. Progenitors of Type Iax SNe*

The reduced explosion energy observed in Type Iax SNe has led to the hypothesis that their progenitor systems may not align with those typically invoked for standard Type Ia SNe. Understanding the explosion mechanisms and progenitor systems of Type Iax SNe is a key area of investigation. Observational characteristics of the bright Type Iax SNe [50,64–67] are consistent with being the outcome of weak deflagrations in C-O white dwarfs [68]. Alternatively, a disk detonation mechanism involving the merger of a white dwarf with a neutron star or black hole has been proposed to explain certain observed traits [69]. For the faintest Type Iax SNe, a broader diversity of progenitor scenarios has been considered. These include mergers between carbon-oxygen and oxygen-neon white dwarfs [70], partial deflagrations in hybrid C–O–Ne white dwarfs [71–73], pure deflagrations in C–O white dwarfs [74], as well as core-collapse mechanisms [75]. Other possibilities include mergers between O–Ne white dwarfs and compact objects such as neutron stars or black holes [76], and electron-capture SNe from super-asymptotic giant branch (AGB) progenitors [77].

Although several models have been proposed, the lack of a substantial sample of well-observed Type Iax SNe hinders any strong assertion of a single progenitor channel or explosion mechanism applicable to the entire class. The detection of outliers within the Type Iax class, such as SNe 2009ku [62] and 2014ck [63], highlights the need for detailed

investigations to better understand the nature of this peculiar subclass of Type Ia SNe. So far, only three Type Iax SNe with intermediate luminosities (SNe 2019muj [78], 2024pxl [79], and 2025qe [80]) have been identified. Given the pronounced heterogeneity observed at both the bright and faint ends of the Type Iax luminosity distribution, it is crucial to closely examine the intermediate-luminosity events. Such analysis may help determine whether they represent a transitional population within a continuous distribution or reflect further diversity in progenitor systems and explosion mechanisms.

## 4. Diversity in Core Collapse SNe of Type IIP/IIL: Observational Insights

The most abundant subclasses of CCSNe are the hydrogen-rich Type IIP/L SNe [81], collectively referred to as Type II SNe. Around 80% [82,83] of Type II CCSNe fall into this category. Both direct detections [84–87] and theoretical models [88,89] suggest that their progenitors are red supergiant stars (RSGs) with extended hydrogen envelopes. Following the explosion, the shock breakout ionizes this envelope, and the subsequent recombination results either in an approximately constant luminosity phase (Type IIP) or a linearly declining phase (Type IIL). Type IIL SNe exhibit a faster decline and a shorter recombination phase than Type IIP SNe which is most likely due to a smaller hydrogen envelope mass and/or a steeper density gradient in the envelope [90–93]. Hydrogen envelope mass alone cannot account for the observed diversity in Type II light curves. Radiative transfer and hydrodynamical models by Hillier and Dessart [94] suggest that interaction with CSM is also a key factor. In some cases, asymmetric CSM distribution may play a role in shaping the observed features of Type IIL SNe [95].

### *4.1. Photometric Evolution of Type II SNe*

Being the most abundant subtype, Type IIP SNe exhibit a diverse range of photometric properties in terms of absolute magnitude ($-18 \geq M_V \geq -14$ mag [4]), plateau length ($\sim$60–140 days [96]), synthesized $^{56}$Ni mass (0.001–0.360 $M_\odot$ [97]), etc. This diversity is caused by the properties of the progenitor, such as the zero-age main sequence (ZAMS) mass, metallicity, ejecta density structure, pre-SN mass loss history, explosion energy, structure, and composition of the surrounding CSM. Type II SNe exhibit significant diversity in their light curves, as evident from the absolute $V$-band light curves of seven events observed with the ARIES telescopes (supplemented by data from other facilities ) (Figure 4). The constant luminosity plateau is more prominent at longer wavelengths (*R, I, NIR*) because the emission in these bands is dominated by the hydrogen recombination front, while the flux in the blue bands (*U, B*) declines more rapidly due to line blanketing and its stronger sensitivity to temperature [4,94,98]. While the majority of Type II SNe exhibit plateau durations between 80 and 120 days, a small but growing sample shows shorter plateaus (less than 80 days), and an extended plateau lasting longer than 120 days has been observed in some cases. The SNe shown in Figure 4 have varied plateau durations: short plateau SN 2020jfo (67 days) [99], normal plateau duration SNe 2014cx (110 days) and 2015cz (114 days) [100], and long-plateau duration SNe 2014cy (125 days), 2015an (130 days), 2015ba (123 days), and 2016B (134 days) [100–103]. The absolute $V$-band magnitudes span a range from $-18$ to $-16$ mag. The inferred progenitor properties, explosion parameters, synthesized $^{56}$Ni mass, and the structure and composition of the surrounding CSM differ across these events.

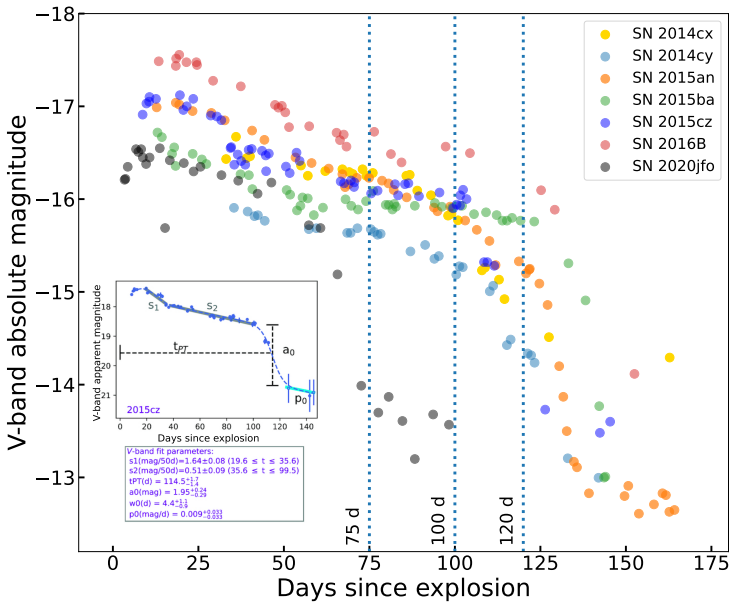


**Figure 4.** The absolute *V*-band light curves of Type II SNe. The distances adopted to estimate the absolute magnitudes are SNe 2014cx (18.5 ± 1.1 Mpc); 2014cy (23.4 ± 1.6 Mpc); 2015an (30.5 ± 0.6 Mpc); 2015ba (34.8 ± 0.7 Mpc); 2015cz (63.7 ± 5.7 Mpc); 2016B (26.8 ± 4.9 Mpc) and 2020jfo (14.51 ± 1.38 Mpc). The three vertical lines at 75, 100, and 120 days represent the typical plateau duration in short-, normal-, and long-plateau SNe. Analytical fit based on [96] is used to extract the light curve parameters such as $a_0$, which indicates the magnitude drop from the recombination phase to the linear tail; $w_0$, which indicates the width of this transition phase (∼6$w_0$); $t_{PT}$, which is a proxy for plateau length; and $p_0$, which constrains the slope before and after the drop. The inset shows the best-fit analytical model to the light curve of SN 2015cz [100] and the best-fit parameters.

### *4.2. Spectroscopic Insights of Type II SNe*

Early phase: The early time spectra of Type II SNe are heavily influenced by their immediate environment. Many massive stars are surrounded by CSM as a result of mass loss during their evolution. When the star explodes, the shock breakout releases high-energy radiation that ionizes the surrounding CSM. As this ionizing radiation passes through and diminishes, the CSM begins to recombine, producing narrow emission lines whose intensity and duration depend on the electron density [104]. These narrow emission signatures in the very early spectra are often referred to as "flash features". Typical flash features include lines of He II, C III, C IV, N IV, N V, and O IV. These flash features can last from a few days SN 2013fs [105] to about a week or so SN 2023ixf [106]—making early observations critical to uncovering these fleeting features. However, if the CSM is optically thick and the shock continues to energize it, the ionization can persist beyond this phase [107]. As the SN ejecta expands and engulfs the CSM, these high-ionization lines fade and transition into lower-ionization features like N III and O III, reflecting the cooling of the circumstellar environment.

Although such features were rarely observed in the past—limited to a handful of events like SNe 1983K [108], 1990E [109], and 1998S [110]—the advent of high-cadence surveys has transformed our ability to capture them. Early-time detections from SNe PTF11iqb [111], 2013fs [105], and 2016bkv [112] reveal that flash features are more common than previously thought. Indeed, ref. [8] found that 18% of SNe observed within five days after explosion exhibit such features, and [113] extended this to 36% for those observed within 48 h. These early emission lines not only trace the immediate pre-explosion environment

but also offer insights into the progenitor's wind velocities, mass-loss rates, and chemical composition [114,115]. The top panel in Figure 5 shows the presence of these "flash features" in five Type II SNe (2013fs [116], 2018lab [117], 2021yja [118], 2023ixf [119], 2024ggi [120]). Some Type II SNe lack strong emission lines and instead exhibit extended spectral features, such as a distinctive asymmetric "ledge-shaped" feature around 4500–4800 Å [118]. The "ledge feature" is marked in the top panel of Figure 5. In SN 2013fs, this feature was interpreted as a broad and blue-shifted component of He II emission arising from the SN ejecta underneath the CSM [116]. Conversely, [118] proposed this feature to arise from the blending of several high ionization lines (e.g., He II, C III, C IV, N IV, and N V) driven by weak CSM interaction. In the absence or disappearance of these flash features, the early spectra of Type II SNe are relatively blue and featureless, as the photosphere lies in the outermost layers of the ejecta.

Photospheric phase: The photospheric phase spectra of Type II SNe mainly consist of the H$\alpha$ profile along with various Fe II lines (middle panel of Figure 5). The prominence of the absorption dip in the P-Cygni[3] profile of the H$\alpha$ line identifies a SN as a Type II, and the ratio of absorption to emission profile correlates with the expansion velocity of the SN ejecta [121]. A small dip on the blue side of the absorption component of H$\alpha$ has been reported in a number of Type II SNe [101–103,122–124]. Ref. [122] referred to these as "complicated P-Cygni profiles", appearing on the blue side of the Balmer lines, while [125] termed this feature as "Cachito". This feature appears either during the early cooling phase or the hydrogen recombination phase up to around 100–120 days since the explosion, with its shape and strength evolving over time. In some Type II SNe, this blueward feature of the H$\alpha$ line has been identified as Si II (6355 Å) [101,123], while some studies suggest it to be a high-velocity component of hydrogen [102,103,126,127].

Ref. [125] argued that if the "Cachito" originates from Si II, its velocity should match that of other metal lines observed at similar epochs. In contrast, if it is associated with hydrogen, its velocity would be comparable to that of the early-time H$\alpha$ line, and a corresponding absorption would also be expected blueward of H$\beta$. The detection of Si II at early times typically indicates a progenitor with a larger radius, which leads to slower ejecta cooling and increases the likelihood of Si II detection. Alternatively, if the feature arises from high-velocity hydrogen, it likely results from the excitation of the outer ejecta layers with photons produced through the interaction of the SN ejecta with the dense wind of an RSG. In such cases, the shape and persistence of the Cachito feature are governed by the density of the surrounding wind [127]. Figure 6 illustrates the presence of the Cachito feature in SN 2014cx, detected in both the H$\alpha$ and H$\beta$ lines.

Nebular phase: As the SN enters the nebular phase, the spectra become emission-dominated due to the optically thin, low-density medium. The H$\alpha$ emission line (6563 Å) is the most prominent in each spectrum, along with detectable features of H$\beta$, Fe II (5169 Å), Na ID (5890, 5896 Å), and the Ca II NIR triplet (8498, 8542, 8662 Å). Several forbidden emission lines, such as [Ca II] (7291, 7323 Å), [O I] (6300, 6364 Å), also become apparent (bottom panel of Figure 5). The [O I] lines are weak in the early nebular phase (e.g., SN 2014cx), but as SN evolves, this line becomes prominent (e.g., the 365-day spectrum of SN 2020jfo). Among other metal features, the Ca II NIR triplet is typically the strongest in the nebular phase; however, in the late-time spectrum of the short-plateau SN 2020jfo, these lines are relatively weak. Instead, this spectrum shows a striking [Ni II] (7378 Å) emission, stronger than [Fe II] (7155 Å)—a feature usually characteristic of low-luminosity Type II SNe.

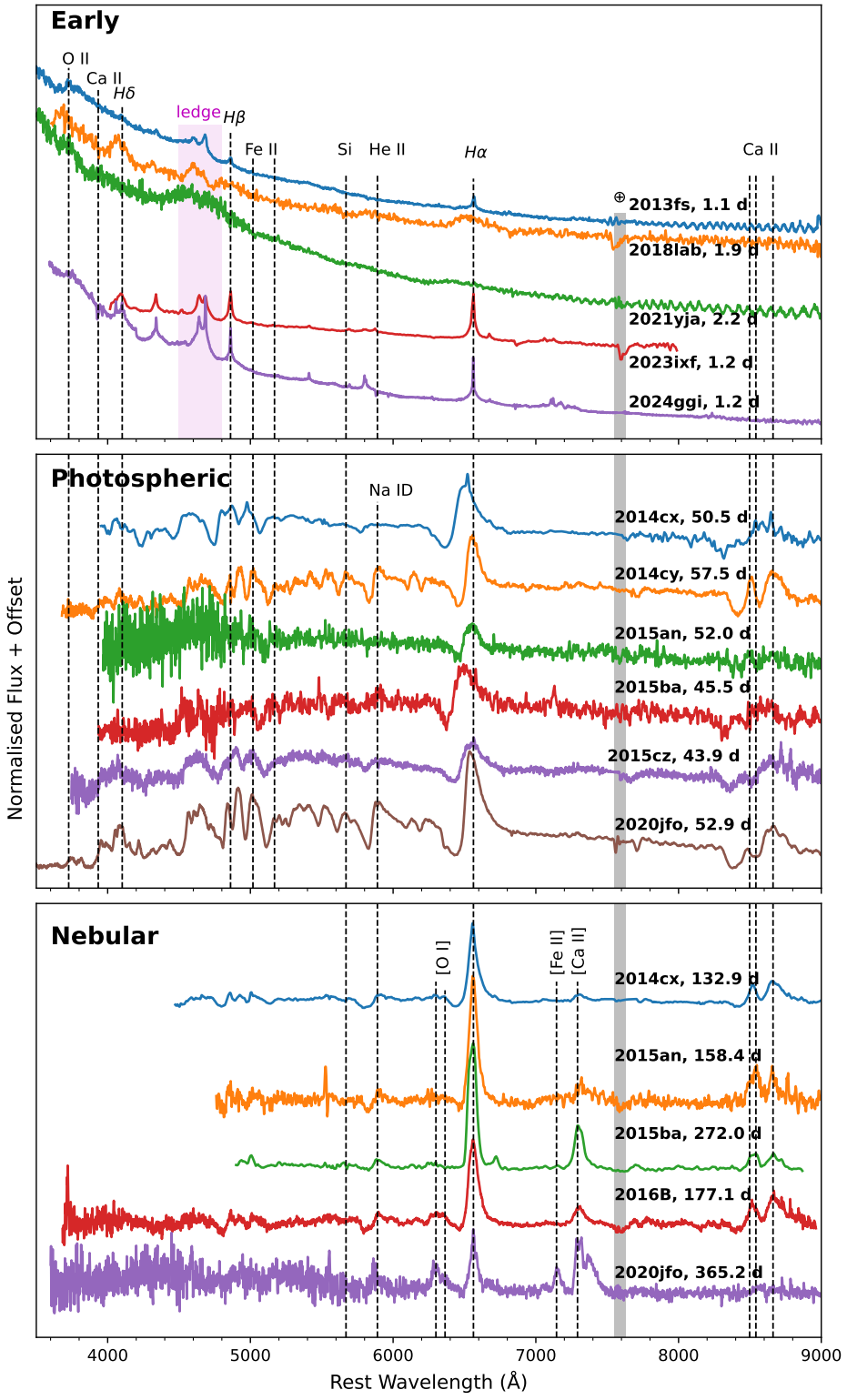


**Figure 5.** (**Top Panel**): The early phase spectra of five Type II SNe. Narrow emission lines ("flash feature") over the continuum are visible. A "ledge-shaped" feature appears around 4500–4800 Å, highlighted in pink color, arising from the blending of multiple high-ionization lines. (**Middle Panel**): The photospheric phase spectra of six Type II SNe at around 50 days are shown. A prominent H$\alpha$ P-Cygni profile, along with other metal lines (e.g., Fe II, Ca II NIR triplet, Na ID), is visible in all spectra. (**Bottom Panel**): The nebular spectra of five Type II SNe at different epochs are shown. A prominent H$\alpha$ emission line is visible in all spectra. Forbidden lines (e.g., [O I], [Fe II], [Ca II]) appear due to the low-density medium.

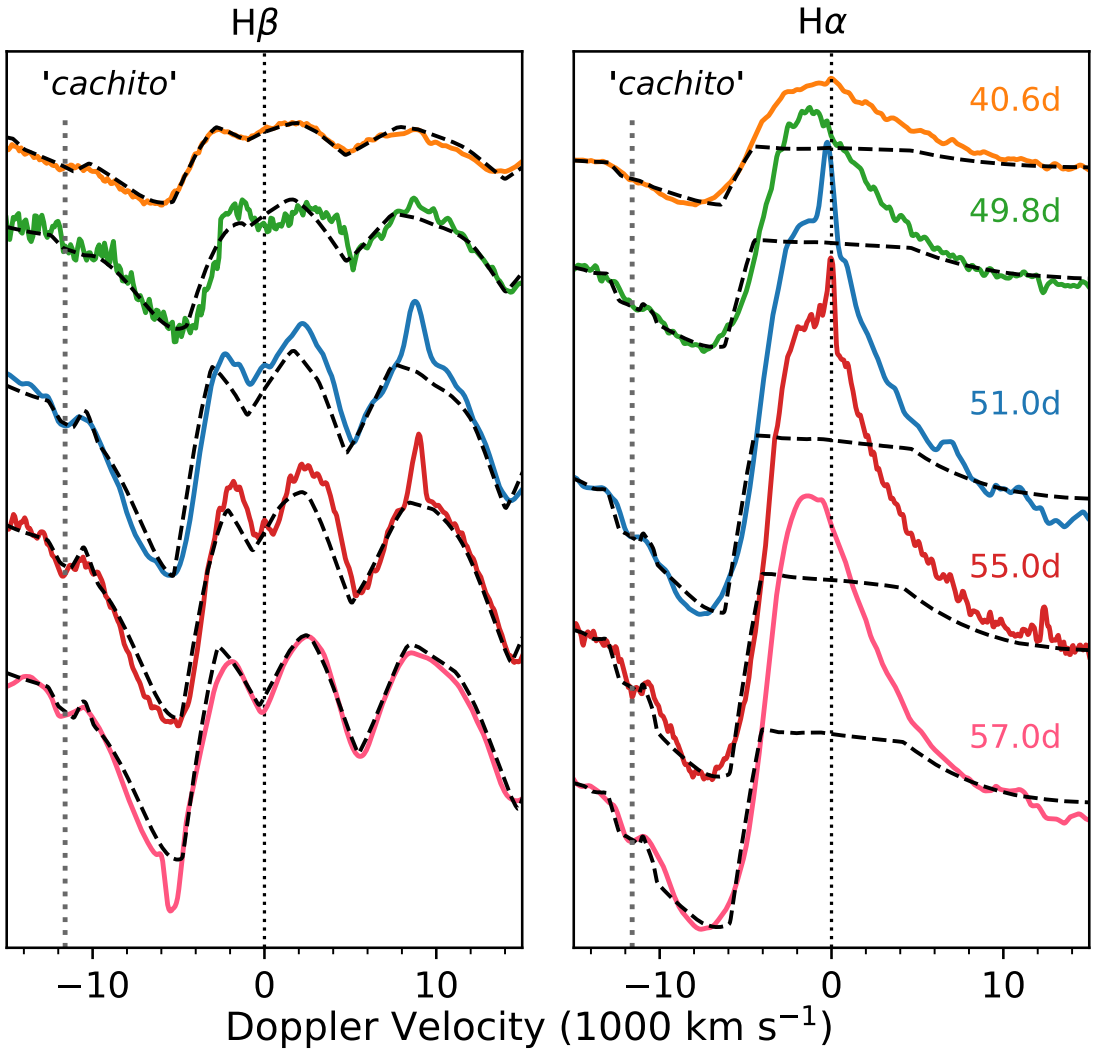


**Figure 6.** "Cachito" feature observed during the photospheric phase of the Type II SN 2014cx [100]. The high-velocity absorption dips on the blue side of H$\alpha$ and H$\beta$ are marked. The dashed lines show the model fits to the spectra, including both a normal and a high-velocity component of H.

The strength of nebular emission lines can be used to constrain the progenitor's ZAMS mass, which is proportional to the mass of the metal core as predicted by stellar evolution models [128]. Ref. [129] demonstrated that the intensity of the [O I] (6300, 6364 Å) doublet in the nebular spectra of Type IIP SNe correlates with the ZAMS mass of the progenitor. They computed model spectra for progenitors of 12, 15, 19, and 25 $M_{\odot}$ across several nebular epochs [130]. By comparing observed spectra with these models at similar epochs, progenitor masses can be constrained. Figure 7 presents such a comparison for the 177 d nebular spectrum of SN 2016B to these models in order to estimate the progenitor mass. The strength of the [O I] doublet (6300, 6364 Å) is best reproduced by the 15 $M_{\odot}$ (ZAMS) model, whereas the 12 and 19 $M_{\odot}$ models under- and overestimate the line strength, respectively [103].

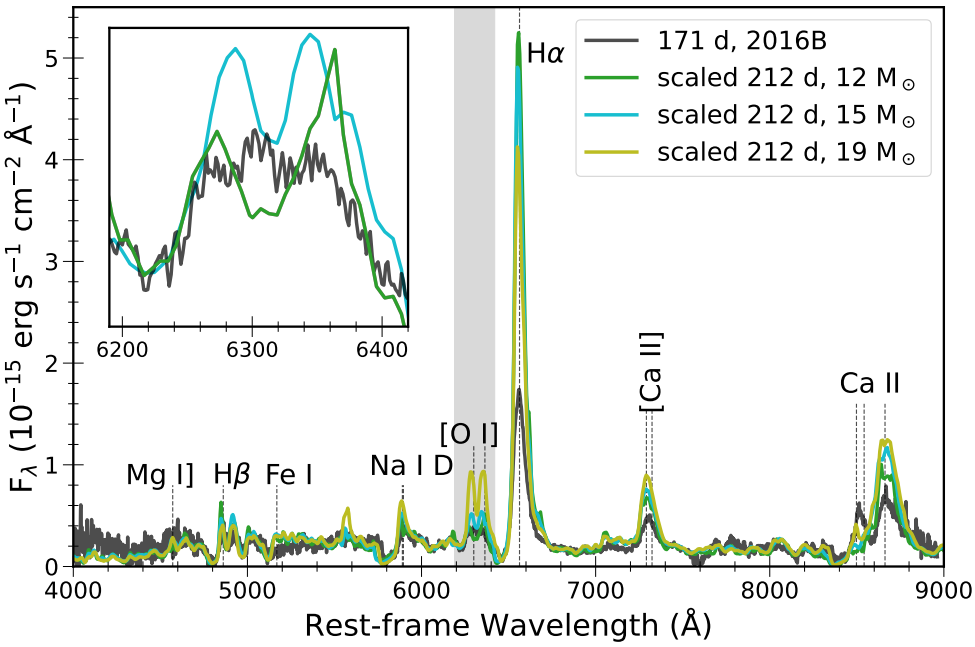


**Figure 7.** Comparison of 177 d spectrum of SN 2016B [103] with the scaled model spectra of 12, 15, and 19 $M_\odot$ from [130].

### *4.3. Type IIP/L Conundrum*

The distinction between Type IIP and IIL SNe was first introduced by [81], based on differences observed in their optical light curves. Subsequent studies with limited sample sizes [4,131,132] further supported the classification into these two subtypes. Approximately 70% of Type II SNe fall under the IIP category, while around 10% are classified as IIL, based on a volume-limited observational sample [82].

While the primary distinction originally focused on light curve morphology—namely, the presence or absence of a plateau—additional observational features have helped to further characterize the two types. Type IIL SNe generally exhibit higher peak luminosities [4,132,133], shorter plateau phases than Type IIP SNe [121,133], and faster ejecta expansion velocities [132]. Moreover, spectroscopic differences include a weaker absorption trough in the H$\alpha$ P-Cygni profile of Type IIL SNe [134,135].

However, rather than representing two distinct populations, [4,5] proposed that these SNe form a continuum of properties. This proposed continuum becomes apparent when examining rapidly declining Type IIP events—those that decline at a rate of about one magnitude per 100 days in the *V*-band during the photospheric phase. These SNe exhibit light curve behaviors that bridge the gap between traditional Type IIP and IIL subclasses [132].

The SNe 2014cx, 2014cy, 2015cz, 2015ba, 2016B, and 2020jfo in our work span a range of observational properties (peak brightness, variable plateau duration, wide range of decline rates, presence of high-velocity hydrogen features and CSM interaction), highlighting the complexity and diversity of the Type II SN population [99,100,102,103]. SN 2014cx shows characteristics of a typical Type IIP SN with a slowly declining plateau, but with a shorter plateau duration. The short plateau and presence of high-velocity hydrogen features hint at CSM interaction and deviation from standard Type IIP behavior. SNe 2014cy and 2015cz exhibit steeper early decline rates, aligning with Type IIL-like light curves. But SN 2016B, although with a steep early decline, displays a longer plateau duration than typical Type IILs. The absence of the expected strong metal features during the plateau phase in SN 2014cy and the presence of high-velocity hydrogen features in SN 2016B further complicate the classification. Persistent high-velocity features in the late-time spectra of

SN 2015ba, a luminous Type IIP with a long plateau, point to CSM interaction. SN 2020jfo with a short plateau, typical of Type IIL SNe but with strong P-Cygni profiles during the plateau phase—more akin to Type IIP behavior.

These SNe illustrate the limitations of a strict Type IIP/L dichotomy and highlight the need for a more nuanced framework for classifying and interpreting Type II SNe in the era of high-cadence, multi-wavelength surveys.

### *4.4. The "Red Supergiant" Problem*

It is important to map the different explosions to their progenitor systems in order to construct a consistent picture of stellar evolution. Early theoretical works [136–138] suggested that Type IIP SNe arise from RSGs. Modern stellar evolution models [89,139] likewise predict that all stars with initial masses $8 \lesssim M \lesssim 25$–$30\ M_\odot$ should end their lives as RSGs and subsequently explode as CCSNe. High-resolution archival images of several Type IIP SNe progenitors have confirmed this [84,87,140–142]. At present, there are ∼30 confirmed cases of RSG progenitors identified in pre-explosion imaging (see review by [143]). However, direct detections of progenitors typically constrain Type IIP SN precursor masses close to the theoretical low-mass limit of core collapse, i.e., $8.5\ M_\odot$ (e.g., SN 2003gd) up to $16.5\ M_\odot$ (e.g., SNe 2009kr, 2012ec) [84,87]. Similar constraints arise from nebular spectral modeling [130,144], though see [145], whereas hydrodynamical models often yield higher upper limits [146–149].

The hydrodynamical and analytical modeling in SN 2015ba suggested a relatively massive progenitor of 24–26 $M_\odot$ [102]; however, its nebular spectra showed only weak oxygen signatures, which is at odds with expectations for such a progenitor mass. This suggests that the relationship between O-core and ZAMS mass may not be strictly linear and that uncertainties in ejecta mixing may play a significant role. Alternatively, the progenitor could have been a merger product, yielding an under-massive core relative to single-star evolution (e.g., [150]). This highlights the difficulty of linking nebular abundances directly to progenitor properties.

Collectively, such findings have raised the so-called "RSG problem", while RSGs of 18–30 $M_\odot$ are known to exist in the Local Group, they appear to be absent as progenitors of observed Type IIP SNe through direct detection. Several explanations have been proposed: a steeper initial mass function (IMF) slope that reduces the expected number of massive stars, enhanced late-stage mass loss redirecting stars into alternative SN channels (IIL, IIn, Ibc), underestimated metallicities leading to higher mass-loss rates and earlier Wolf–Rayet (WR) transitions, dust obscuration concealing massive progenitors in pre-explosion imaging, and the possibility of failed SNe through direct black hole formation [84,151].

More recently, however, the significance of the RSG problem has been questioned. Ref. [151] used Bayesian simulations to suggest an upper cutoff of as low as $15.7 \pm 0.8\ M_\odot$. Ref. [152] provides a revised cutoff of $19^{+4}_{-2}\ M_\odot$, consistent with observational samples, and does not strongly support a missing high-mass RSG population. Likewise, ref. [153,154], in their latest progenitor analyses, conclude that current evidence is insufficient to confirm the problem, given the small sample size, observational biases, and the possibility of failed SNe. While the existence of massive RSGs in the Local Group is undisputed, whether they contribute significantly to the observed SN population remains an open question.

## 5. The Stripped Envelope Group of CCSNe

Stripped-envelope SNe (SESNe) are core-collapse explosions from massive stars that have lost part or all of their outer envelopes prior to collapse. They comprise Type IIb, Ib, and Ic SNe, classified based on the presence or absence of hydrogen and helium in their spectra [1,155]. Type IIb SNe show transient hydrogen features that fade to reveal

helium-dominated spectra, indicating progenitors that retain a thin residual hydrogen envelope. Type Ib SNe lack hydrogen lines but display strong helium features, while Type Ic SNe exhibit neither hydrogen nor helium lines, reflecting more extreme stripping.

Observationally, SESNe account for approximately 30–35% of all CCSNe, with typical relative fractions of ∼10% for Type IIb, ∼10–15% for Type Ib, and ∼15–20% for Type Ic [82,156,157]. Their progenitors are thought to be massive stars ($\gtrsim$8 $M_\odot$) that have undergone significant mass loss either through strong stellar winds, as in WR stars, or via binary interaction where a companion star strips away the outer hydrogen and helium layers [158,159]. Type IIb progenitors are often identified as yellow or red supergiants with thin hydrogen envelopes, whereas Type Ib and Ic SNe are more consistent with compact helium or CO cores, respectively, with Type Ic involving the most extensive stripping [84,159,160].

Understanding SESNe is crucial for constraining the final evolutionary pathways of massive stars, binary interaction physics, and their role in enriching the interstellar medium with heavy elements. Additionally, broad-lined Type Ic SNe have been directly linked to long-duration gamma-ray bursts (GRBs), connecting SESNe to the most energetic stellar explosions in the Universe [161].

### *5.1. Light Curve and Spectral Characteristics of SESNe*

The SESNe studied in [162–164] reveal a continuum of photometric properties. At the fainter end, some events lack an early cooling peak yet display plateau-like features at later times. SN 2015as (Type IIb) is an example, reaching a peak *B*-band magnitude of ∼−16.8 mag with a rise time of ∼22 days, showing no distinct early cooling peak but developing a mild plateau between 70 and 100 days before declining gradually. At the brighter extreme, certain SNe are more luminous at the peak and evolve rapidly. SN 2015ap (Type Ib) attained $M_V \sim -18.0$ mag with a fast decline, requiring both radioactive $^{56}$Ni decay and magnetar input to reproduce its luminosity. SN 2016P (Type Ic) peaked at $M_V \sim -17.5$ mag and exhibited a hybrid-powered light curve. Between these extremes lie transitional objects that show slower-evolving light curves with intermediate luminosities. SN 2022crv (Type IIb/Ib) peaked at $M_V \sim -17.8$ mag and evolved more gradually than SNe 2015ap and 2016P. Collectively, these events cover a wide range in luminosities (–16.8 to –18.0 mag), rise times, decline rates, and the presence or absence of early cooling peaks and plateaus, reflecting differences in progenitor envelope stripping, explosion energies, and the role of CSM.

The spectral properties of these SESNe reinforce this continuum. Some Type IIb SNe begin with strong hydrogen features that fade as helium emerges: SN 2015as initially displayed Balmer lines, which weakened with time, while He I P-Cygni features became prominent after ∼30 days, marking its transition toward an Ib-like spectrum. Other SNe show persistent helium and heavier-element features. SN 2015ap, for instance, exhibited early He I, Fe II, Mg II, Na I, and Si II lines, while its nebular spectra revealed asymmetric [O I] emission. Transitional behavior is again exemplified by SN 2022crv, which displayed H$\alpha$ absorption at early times that disappeared after maximum light, while He I features simultaneously strengthened, confirming its Type IIb to Ib evolution. Figure 8 (left panel) shows the representative spectral evolution of Type IIb and Ib SNe. The spectral features highlight that Type IIb and Ib are linked by a continuum of hydrogen and helium envelopes, i.e., both have some amount of remaining hydrogen and helium. Classical Type Ic events lack helium entirely: SN 2016P showed no He features, with spectra dominated by Fe-group absorption lines and prominent O lines (Figure 8 right panel). Late-time nebular spectroscopy provides additional progenitor constraints. For e.g., MASTER OT J120451.50+265946.6 (M12045), a rapidly declining but spectroscopi-

cally normal SN, exhibited nebular-phase signatures consistent with a massive progenitor ($\sim$20 $M_\odot$ [165]).

Both photometric and spectroscopic observations reveal a considerable diversity within the SESNe class, reflecting the underlying variations in their progenitor properties, explosion mechanisms, and circumstellar environments.

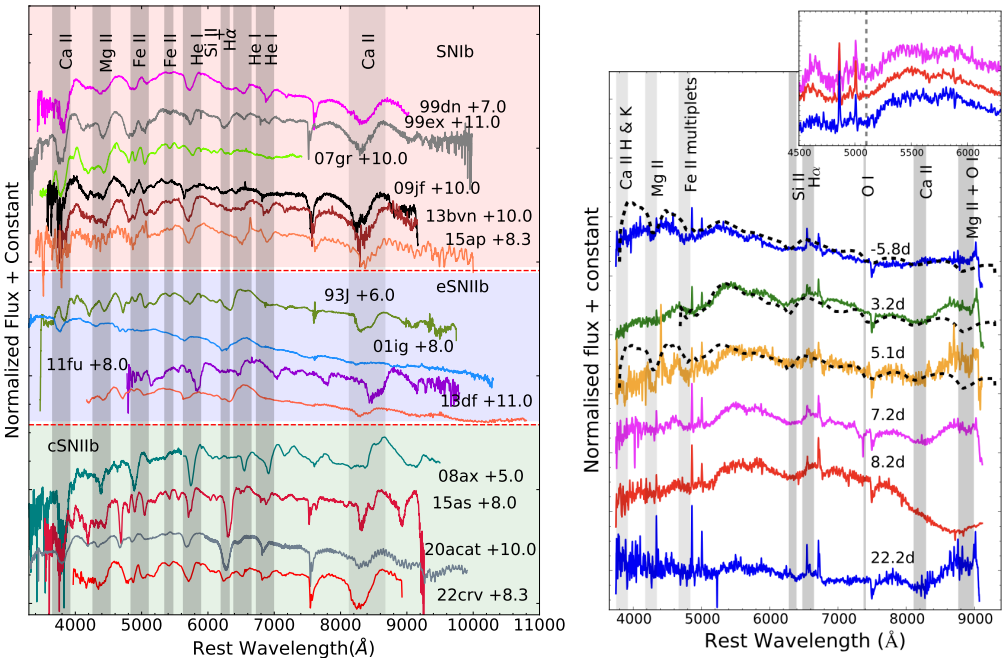


**Figure 8.** (**Left panel:**) Spectra of Type IIb and Type Ib SNe a few days after peak luminosity [164]. (**Right panel:**) Spectral evolution of a Type Ic SN 2016P [163].

### *5.2. Progenitor Properties*

Combined analyses of the SESNe place strong constraints on their progenitor systems, revealing a wide range of evolutionary pathways. Moderately stripped progenitors retaining thin hydrogen envelopes over a compact helium core could be one channel (e.g., SN 2015as). The oxygen mass estimated from the nebular [O I] emission line indicates a $\sim$15–20 $M_\odot$ main-sequence star or a lower-mass WR star as the progenitor of SN 2015as [162]. At the other extreme end, highly stripped helium or CO cores appear to give rise to the brighter, faster-evolving Type Ib and Ic SNe with progenitor masses between $\sim$12–20 $M_\odot$ (e.g., SNe 2015ap and 2016P). An additional energy input, like a magnetar, is required to model the light curves of such SNe (e.g., SN 2015ap [163]). Transitional Type IIb/Ib SNe represent another pathway, where progenitors retain only extremely thin hydrogen layers and show evidence for active mass loss (e.g., SN 2022crv), in line with compact binary-stripped progenitors [164].

Overall, these studies underscore the diversity of SESN progenitors—from moderately stripped supergiants to heavily stripped helium or CO cores—and highlight the interplay of binary mass transfer, stellar winds, and, in some cases, magnetar central engines in shaping their final explosions and observed diversity.

### *5.3. Stripped-Envelope SNe: Global Properties and Population Studies*

Large-sample studies have greatly advanced our understanding of the diversity and shared characteristics of SESNe. Ref. [166] conducted the first systematic analysis of SESN light curves, finding that Type Ib and Ic exhibit comparable peak luminosities ($M_R \sim$ –17.9 mag) and fast rise times ($\sim$10–20 days), whereas Type IIb SNe are typically fainter and evolve more slowly. Spectroscopic comparisons further revealed that while Type

Ib and Ic share many features, Type Ic SNe consistently lack helium signatures even in high signal-to-noise spectra, pointing to a genuine physical absence rather than observational limitations [167]. Building on this, ref. [168] analyzed spectral velocities and line strengths in a larger sample, showing that Type Ic SNe tend to have higher Fe II velocities, indicative of systematically greater kinetic energy per unit mass. Several other sample studies of SESNe have reported that they constitute about 30% of all core-collapse SNe, with Type Ic being slightly more prevalent than Ib, and they tend to occur in environments with higher star formation and lower metallicity compared to Type II SNe [156]. Type Ic-BL SNe exhibit the highest kinetic energies among core-collapse types [169], while SESNe show broad peak magnitude distributions with significant intrinsic scatter across subtypes [170].

Collectively, these studies reveal that SESNe form a diverse but continuous class, with systematic differences in envelope stripping extent, kinetic energies, and host environments, pointing toward progenitor channels that include both single WR stars and binary-stripped helium stars across a range of metallicities.

## 6. The Interacting Group of CCSNe

The observational hallmark of strong interaction with the CSM is the presence of narrow emission lines in the spectra. This feature led to the classification of Type IIn SNe [171], now understood as SN ejecta interacting with dense, hydrogen-rich CSM. Interaction with the helium-rich, hydrogen-poor CSM, characterized by narrow He I lines and absence of hydrogen, is classified as Type Ibn SNe SN 2006jc [24]. SNe that interact with H- and He-free CSM would typically exhibit narrow C/O features and no broad ejecta lines at early times and are classified as Type Icn SNe SN 2019hgp [25]. Very recently, Schulze et al. [172] discovered an SN showing interaction signatures of narrow Si and S, labeled as Type Ien SN, leaving the Idn title as a placeholder for SNe showing interaction signatures of O/Mg/Ne [173]. Interacting SNe constitute about 10% of the CCSNe [174], which makes them rare and interesting. Additionally, interacting SNe show significant diversity among the established subclasses and also within the subclasses themselves.

Type IIn SNe progenitors are often associated with LBVs or massive RSGs undergoing episodic mass loss or binary-induced outflows [7,10]. Type Ibn SNe events are typically linked to WR stars or He-rich stripped-envelope progenitors with compact winds [175]. Type Icn SNe are most consistent with either ultra-stripped binaries or massive WR stars with C/O-rich envelopes [176]. Mass loss in massive stars—central to CSM formation—is influenced by factors like luminosity and metallicity [7]. However, winds are often clumpy and variable, complicating predictions of mass-loss rates [177]. In addition to steady winds, episodic eruptions, such as the historical outburst of $\eta$-Carinae, may result from instabilities or binary interactions. In particular, a large fraction ($\sim$70%) of massive stars are in binary systems, underscoring the importance of binary evolution in shaping the CSM structure [178].

### *6.1. Light Curve Characteristics of Interacting SNe*

The light curves of Type IIn SNe are primarily powered by shock interaction, which converts the kinetic energy of ejecta into electromagnetic radiation. Therefore, Type IIn SNe are generally much brighter than regular Type II SNe with comparable explosion energies. Their luminosity is directly influenced by the density and extent of the CSM, and therefore, the light curves vary widely. High-density CSM can give rise to superluminous luminosities, as seen in the case of SN 2006gy [179], and ASASSN-14il [10]. If the CSM extends up to very large distances, the interaction can keep the SN luminous for very long times, as seen in the cases of SNe 2010jl [180] and 2012ab [181]. In addition to this, since the radial density gradient of the CSM can have significant variations, the shapes of the

light curves can vary drastically, with some events showing plateau-like features in their light curves (e.g., SN 2012ab [181], ASASSN-14il [10]), bumps in the light curve (e.g., SN 2009ip [182], ASASSN-14il [10]), and even double-peaked light curves (e.g., SN 20009ip [182]).

In contrast, the light curves of Type Ibn and Icn SNe are less heterogeneous, with rapid evolution. Type Ibn SNe show a rise time of $<$15 days and fast decline ($\sim$0.05–0.15 mag day$^{-1}$), and Type Icn SNe show even faster evolution [175,176].

Precursor emission from pre-SN outbursts as a result of late-time instabilities in the progenitors is also seen in many interacting SNe like SNe 2006jc, 2009ip, 2021foa, 2023vbg [24,182–184].

### *6.2. Spectral Characteristics of Interacting SNe*

The early time spectra of interacting SNe are dominated by blue continuum and narrow emission lines on top of broad Lorentzian wings. The narrow lines originate from the ionized CSM ahead of the shock front and trace the velocity and composition of the slow-moving CSM. Type IIn SNe usually show narrow lines of H and He. While Type Ibn SNe shows little to no H, it shows narrow He lines. Congruently, Type Icn SNe show trace He but narrow lines of C/N/O. These narrow lines often show a P-Cygni profile characteristic of an outflow. The high electron scattering depths in the CSM at early times give rise to the broad wings [185]. Rapid follow-up observations have revealed that interacting SNe also show early high-ionization flash features tracing the immediate CSM. Narrow emission lines from He II, C III, N III, and O IV, lasting only hours to days, provide direct constraints on progenitor winds, mass-loss rates, and chemical composition [8,9,113].

When the photosphere recedes from the ionized CSM ahead of the shock front, the spectrum slowly morphs to show signatures of the interaction region and the inner ejecta. The cold-dense shell (CDS) formed between the forward and the reverse shock usually stays optically thick during this period [186]. In this case, the line profiles are dominated by emission from this thin shell expanding at a few thousand km/s, showing a flat-topped profile, often with the red side showing a flux deficit due to obscuration from the photosphere [187]. The ejecta signatures manifest in broad emission lines (sometimes P-Cygni profiles) and Ca II triplet emission, and later, other heavy elements show up [10].

Ideally, the ejecta signatures should show up once the CDS has become optically thin, which is expected much later than the peak luminosity. However, in many SNe, the CDS and the ejecta signatures are revealed simultaneously, indicating asymmetry in the CSM, which allows direct line-of-sight to the ejecta, as seen in the cases of SNe 2012ab, ASASSN-14il, and 2021foa [10,181,183]. Figure 9 shows the representative spectra taken near peak luminosity for some of these SNe.

With the increasing number of well-studied interacting SNe, the emerging consensus suggests that asymmetry in the CSM geometry may be a ubiquitous feature among these. This is not unexpected, however, if we consider the fact that a significant fraction of all stars are part of a binary system. If we consider an asymmetric disk-like CSM expected from mass loss influenced by binary interactions, we can explain the observed properties of SNe 2012ab, ASASSN-14il, and 2021foa as special cases of this geometry, as shown in Figure 10. In SN 2012ab, a high-velocity P-Cygni H$\alpha$ line from ejecta is visible from very early times, as there is no line-of-sight CSM to obscure the ejecta signatures. ASASSN-14il demonstrates the same, but the early high-velocity ejecta is hidden due to interaction with a second component of CSM that persists in the line of sight. In the case of SN 2021foa, the highest velocity ejecta is hidden by the dense CSM, and this line-of-sight CSM also gives rise to narrow P-Cygni lines. Ref. [188] analyzed a sample of Type IIn SNe with spectropolarimetric data and found many cases where asymmetry in CSM was accompanied by low

polarization, which can be naturally explained as a disk-like CSM structure with face-on symmetry towards the observer.

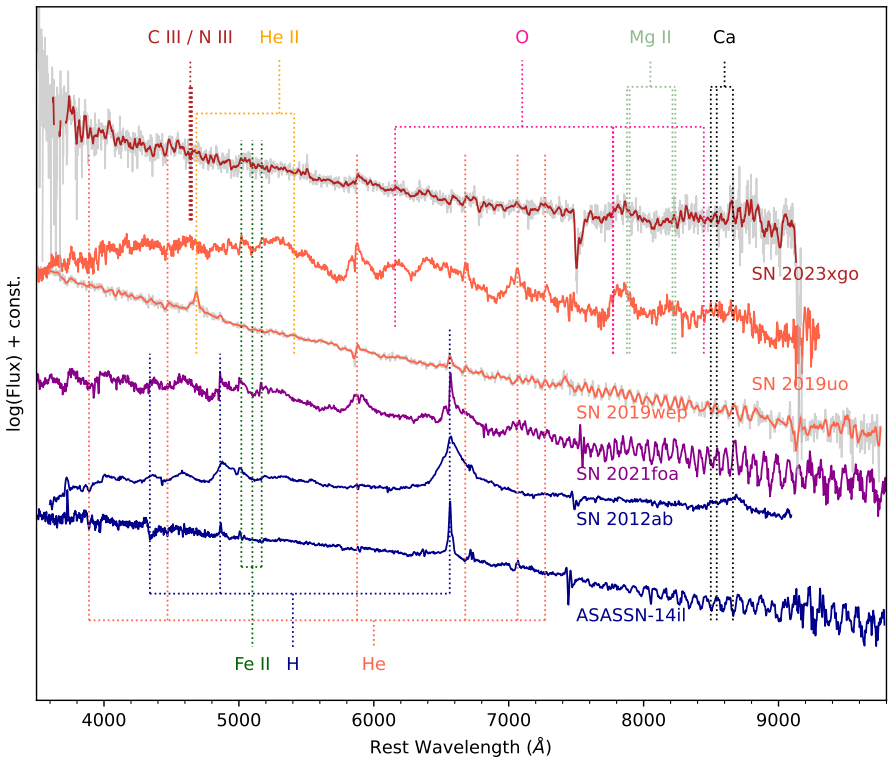


**Figure 9.** Representative spectra near peak luminosity from different subclasses of interacting SNe are plotted (ASASSN-14il—ref. [10]; SN 2012ab—ref. [181], SN 2021foa—ref. [183], SN 2019wep—ref. [189], SN 2019uo—ref. [9], SN 2023xgo—ref. [190]). Type IIn SN are shown in 'blue', IIn/Ibn are shown in 'purple', 'Ibn' are shown in 'orange', and Ibn/Icn are shown in 'brown'. These events show great diversity among their spectral features. The spectrum of ASASSN-14il and SN 2021foa suffers from imperfect fringing correction at $\gtrsim$8000 Å.

Even in cases of spherical symmetry, the CSM may show complex structure in the radial direction, as seen in the case of SN 2023vbg. It shows dual H$\alpha$ components ($\sim$500 and 3000 km s$^{-1}$) [184], interpreted as evidence for an inner dense CSM shell and a more extended outer envelope—further underscoring the variety in pre-SN mass-loss structures.

Overall, it is clearly seen that the interacting SNe show significant diversity among the established subclasses and also within the subclasses themselves. These studies highlight strong ejecta–CSM interactions, asymmetric geometries, and eruptive and possibly binary-influenced mass loss typical of interacting SNe in line with growing consensus.

### *6.3. Transitional Events*

With the observed diversity in interacting SNe, it is not unexpected that we find SNe that do not completely adhere to a particular subclass. These events may either transition from one class to another or show features characteristic of different classes at different times in their evolution, serving as a link between the different subclasses.

Ref. [183] found that SN 2021foa shows similarities with both Type IIn and Type Ibn SN. Many Type IIn SNe also show narrow/intermediate width He emission, but in SN 2021foa the He I 5876 line luminosity was found to be comparable (lower by a factor of $\sim$2) to the H$\alpha$ line velocity. Line strength comparison with a sample of Type IIn and Type Ibn SNe showed that it is intermediate to both these classes, showing similarities to either of the classes at different times in its evolution. They explain this behavior as a combination

of having an asymmetric CSM distribution and a progenitor intermediate between an LBV and a WR star.

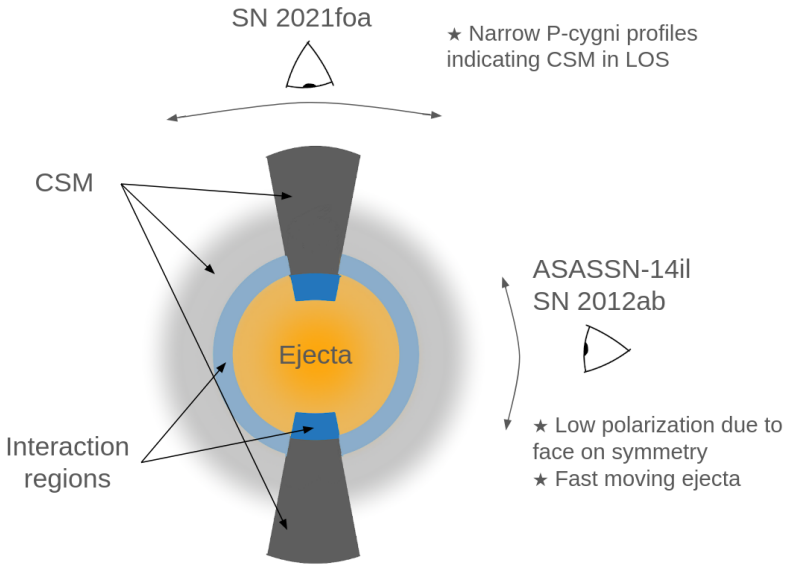


**Figure 10.** This figure shows a cross-section of a system where the SN ejecta (yellow) is interacting (blue) with a disk-like CSM (gray). This illustration shows how similar geometric configurations may give rise to different line shapes in the spectrum. Low polarization of ASASSN-14il despite the asymmetric CSM suggests a face-on symmetry of the CSM. SN 2012ab shows very high velocity ejecta at early times, indicating direct line-of-sight (LOS) to the ejecta. SN 2021foa shows narrow P-Cygni lines as the photosphere recedes inwards in the LOS CSM.

Ref. [190] have shown that SN 2023xgo is a faint, rapidly evolving SN that displays characteristics bridging Type Icn and Type Ibn classes. Early spectra showed unusually strong C III emission, among the most prominent observed in any SN, which faded by peak light (∼5 days post-discovery) as narrow He I P-Cygni lines emerged, resembling typical Type Ibn features. Its peak absolute magnitude was $\sim -17.65$ with a fast decline rate (∼0.14 mag/day), placing it at the faint–fast end of the Ibn/Icn population. Light curve modeling indicated interaction with a compact, stratified CSM, implying variable pre-SN mass-loss rates ranging from $\sim 10^{-4}$ to a few $M_\odot$ $yr^{-1}$ in denser regions. The inferred low ejecta mass (∼0.12 $M_\odot$) and Ni mass (∼0.04–0.05 $M_\odot$) suggest a stripped helium-star progenitor, possibly in a compact binary system. SN 2023xgo provides rare evidence of transitional behavior between Type Icn and Ibn SNe, shedding light on diverse mass-loss mechanisms in the final stages of massive star evolution.

The study of these peculiar interacting SNe suggests that the classification of Type IIn, Ibn, and Icn is not as strict as previously thought, and there are SNe that show intermediate and/or transitional properties. Interacting SNe are a diverse class of explosions that are caused by explosions of not only massive LBV/WR stars but also ultra-stripped stars in binaries, surrounded by H/He/C-rich CSM, often asymmetric. The observed diversity in interacting SNe reflects a variety of progenitor channels and mass-loss mechanisms.

### *6.4. Heterogeneity in Interacting SNe and Their Progenitors*

Studies of interacting SNe reveal both shared and distinct properties across these classes. Ref. [191] analyzed a large sample of 487 Type IIn SNe, showing wide diversity in peak luminosities ($\sim 10^{42}$–$10^{44}$ erg $s^{-1}$) and timescales (20–300 days above half-maximum). Their analysis revealed a bimodal distribution: a luminous–slow group with high radiated energies ($\sim 10^{50}$ erg) and a faint–fast group ($\sim 10^{49}$ erg), with potential hints of a third subgroup. Spectral diversity is also evident, as some Type IIn events maintain strong,

narrow Balmer lines for months, while others display only short-lived electron-scattering features, implying different mass-loss rates and CSM configurations. These results suggest multiple progenitor pathways, including LBVs with eruptive mass loss and super-AGB stars, each producing distinct CSM properties and explosive interactions.

In contrast, ref. [175] studied ∼25 Type Ibn SNe, finding remarkably homogeneous light curves with rapid rises (<15 days) and declines (∼ 0.05–0.15 mag day$^{-1}$), peaking near –19 mag, driven by interaction with compact, He-rich CSM shells. However, spectra revealed significant diversity: some showed narrow P-Cygni He I profiles indicating dense, slow-moving winds (∼200–2000 km s$^{-1}$), while others were dominated by broader emission lines, implying varying CSM density and geometry. Transitional Type Ibn/IIn events with residual H lines further point to a continuum in progenitor types and pre-SN mass-loss modes, likely involving both WR stars and LBV-like progenitors.

Meanwhile, ref. [176] examined four Type Icn SNe, revealing peak luminosities comparable to Type Ibn/IIn but with distinct early-time spectra dominated by strong carbon and oxygen lines rather than helium or hydrogen. Light curves showed fast rise and decline similar to Type Ibn, with ejecta masses $\leq$2 M$_\odot$ and Ni masses $\leq$0.04 M$_\odot$, suggesting multiple progenitor channels: some events likely arise from ultra-stripped low-mass helium stars in binary systems, while others may originate from more massive WR progenitors. The diversity in host environments—from star-forming galaxies to low-metallicity dwarfs—further supports this heterogeneity.

These studies suggest that interacting SNe share a unifying mechanism of ejecta–CSM interaction, producing luminous, often rapidly evolving light curves, but differ in progenitor structure, mass-loss history, and CSM composition. Type IIn SNe show the broadest diversity in luminosity and timescale due to hydrogen-rich dense CSM shells with varying extents. Type Ibn SNe display homogenous photometric evolution but diverse helium-dominated spectral features, suggesting different wind structures or viewing angles, while Type Icn SNe represent a rarer class with strong carbon features, low ejecta mass, and multiple evolutionary origins. Together, these samples underline the rich diversity of stripped-envelope massive stars and their final complex mass-loss phenomena before core collapse.

## 7. Discussion and Conclusions

In this review, we discuss the optical properties of the different classes of SNe. The two important SN observables are the light curves and spectra, delving great insights into their explosion mechanisms and progenitors. The combination of high cadence, multi-wavelength observations, and modeling tools has revolutionized our ability to map SN diversity to progenitor properties and explosion physics. We discuss the observing facilities available and the selection of targets for the follow-up observations. The SN monitoring program, summarized in this work, is one of the primary observing programs at ARIES. This program would not have been successful without the coordinated follow-up campaigns across different telescopes worldwide. Our observational campaign reveals considerable diversity in the photometric and spectroscopic properties of all types of SNe.

### *7.1. Assessment from SNe Observables: Light Curve and Spectra*

Type Iax SNe, a relatively new subclass of thermonuclear explosions, are considered as low-luminosity cousins of normal Type Ia SNe. They show marked deviations from normal Type Ia SNe in both light curves and spectra. The most distinctive feature is the absence of NIR secondary peaks, lower luminosities, and varied post-maximum behaviors in Type Iax SNe, which suggest distinct explosion mechanisms and progenitor systems.

In Type II SNe, light curve behaviors range from slowly declining plateaus typical of Type IIP (e.g., SNe 2014cx, 2015ba) to rapidly declining events resembling Type IIL SNe (e.g., SNe 2014cy, 2015cz). Plateau durations span from as short as ∼67 days (SN 2020jfo) to as long as ∼123 days (SN 2015ba), indicating a wide range of hydrogen envelope masses. Despite their early decline, several SNe exhibit strong H$\alpha$ absorption, challenging the classical IIP/IIL classification. Spectroscopic analyses further highlight this diversity. Features such as the high-velocity Cachito feature (e.g., SN 2014cx, SN 2015ba) point to possible CSM interaction. Spectral modeling infers a wide range of progenitor masses (e.g., 12–26 $M_{\odot}$), with discrepancies in oxygen line strengths hinting at complex mixing and explosion mechanisms. While traditional subclassifications (IIP/L) offer a framework, our results indicate that many events exhibit hybrid characteristics, highlighting that both light curve evolution and spectral features are to be considered while classifying the SNe. These studies also suggest a continuum in light curve shapes, spectral indicators, explosion parameters, and progenitor systems rather than discrete types.

Large-sample studies of SESNe (Type IIb, Ib, and Ic) reinforce their collective diversity. Photometrically, Type Ib and Ic exhibit similar peak luminosities and fast rise times, while Type IIb SNe are typically fainter and slower. Although with diverse light curves and spectroscopic characteristics, SESNe could be a continuous class with varying degrees of envelope stripping, kinetic energies, host metallicity, circumstellar environments, and explosion mechanisms.

The interacting SNe (Type IIn, Ibn, and Icn) constitute a small population amongst the CCSNe. They are luminous in comparison to other types of SNe and show a great diversity among the different interacting subclasses and also within a subclass. This also hints that the different classes of interacting SNe are not strictly separate but display intermediate and/or transitional properties. The most favored progenitor scenarios are the explosions of massive LBV/WR stars and ultra-stripped stars in binaries, surrounded by H/He/C-rich CSM, often asymmetric.

### *7.2. CSM Interaction in SNe*

As discussed in the previous sections, CSM is ubiquitously present around SNe and can significantly impact the dynamics of the explosion and, in turn, the photometric and spectroscopic properties of SNe. Mass loss in the final phases of stars is still not a well-understood phenomenon. Mass loss and CSM formation can have many channels, such as line-driven winds, episodic eruptions, binary interactions, etc., and it is heavily influenced by ZAMS mass, luminosity, metallicity, and the environment of the progenitor star. However, we can broadly categorize the effects of CSM into the following categories.

Flash features: These features arise when low-density CSM, immediately adjacent to the progenitor star, becomes ionized by the shock breakout in the SN ejecta. When the CSM recombines, flash features are observed as narrow emission lines of high ionization species, e.g., He II, C III, C IV, N IV, N V, and O IV. These features are very transient in nature (timescales of a few hours to a few days), as the nearby CSM is quickly swept up by the SN ejecta.

Short-lived interaction: If the density and extent of CSM surrounding the progenitor star are higher than what is seen for flash features, the SN ejecta shock interacts with the dense CSM. This can give rise to narrow lines with electron-scattering wings typically seen in interacting SNe, and it can give a significant boost to the SN luminosity (e.g., SNe 1998S [110] and 2023ixf [119]). In some peculiar geometries of CSM, the spectroscopic signatures of the interaction may remain hidden to the observer, but the interaction actively enhances the luminosity of the SN, especially at the early phases (e.g., SN 2019nyk [192]).

The SN explosion morphs back into a regular SN resembling its class once the CSM is swept up.

Strong long-lasting interaction: When the CSM is dense and spatially spans up to large distances from the progenitor, the SN explosion shows signs of interaction throughout its evolution, lasting years and even decades, as seen in interacting SNe.

The CSM may not necessarily be spherically symmetric. Late-time eruptions seen in massive stars can have a large degree of asymmetry associated with them. In addition, other internal and external factors, such as rotation in the progenitor star and binary interactions, can introduce asymmetry in all channels of CSM formation. These asymmetries can give rise to a variety of interesting features, such as peculiar line profiles, hidden CSM-interaction, etc.

### *7.3. Next Generation Perspectives on Transient Science*

The upcoming Rubin Legacy Survey of Space and Time (LSST) promises to revolutionize transient astrophysics by enabling systematic, high-cadence monitoring of the entire southern sky down to $r \sim 24.5$ mag per visit [193]. Its unprecedented depth, large field of view, and regular revisit cadence will yield millions of transient detections, including rare and rapidly evolving transients such as Type Iax, ultra-stripped SNe, exotic interacting classes (Type IIn/Ibn/Icn), Ca-rich gap transients, and Fast Blue Optical Transients (FBOTs), revealing their rates, progenitors, and links to exotic endpoints such as magnetars or tidal disruptions.

In Type Ia SNe cosmology, LSST's vast sample will refine luminosity relations, host dependencies, and extinction laws, improving distance calibrations [193–197]. Crucially, it will identify transitional events bridging classifications, challenging current taxonomies, and refining stellar evolution pathways.

LSST will advance the detection of pre-SN emission across various SN types. SN 2020tlf (distance 30 Mpc) is the first normal Type IIP/L SN for which precursor emission has been detected at $M_r \approx -11.5$ [198]. Although such precursor activity is theoretically expected to be common in Type IIP/L SNe, it has remained largely undetected, typically falling below the sensitivity limits of current surveys such as ZTF and ATLAS. With LSST, it will be possible to detect pre-SN emission as faint as $-11$ mag in Type IIP SNe out to distances of 100 Mpc. At $D = 100$ Mpc, a single-visit $5\sigma$ depth of $i \simeq 24.0$ implies $M_i = -11.0$ mag, appropriate for red RSG-like precursors [193]. Wave-driven outburst models for RSGs predict luminosity enhancements corresponding to $M_{\rm bol} \sim -10$ to $-12$ [199], consistent with this threshold. The progenitors of Type IIP SNe, likely RSGs, are expected to undergo intense mass loss during their final evolutionary stages. These observations will significantly enhance our understanding of the final stages of stellar evolution and the processes driving mass loss and instability in massive stars.

For stripped-envelope and interacting SNe, LSST's ability to capture early light curve phases will constrain progenitor radii, explosion energies, and mass-loss histories by revealing features such as shock breakout and cooling tails [200]. The vast homogeneous samples of SESNe will enable robust statistical studies of progenitor channels, metallicity dependencies, and explosion diversity across cosmic time. Moreover, rapid follow-up spectroscopic observation upon discovery of transients will allow for the detection of fleeting flash ionization signatures in the hours to days post-explosion. This will provide direct probes of immediate circumstellar environments [201].

LSST will readily detect SNe in Coma ($D \sim 100$ Mpc): a normal SN Ia ($M_B \approx -19.3$) has $m \approx 15.7$ and typical core-collapse SNe ($M \approx -17$) have $m \approx 18$. However, we want to remark that LSST is seeing-limited (median FWHM $\sim 0.7''$ [193]), so at 100 Mpc, where $1'' \approx 485$ pc, the PSF spans $\sim 340$ pc—far above stellar scales. Individual stars are

thus unresolved: even luminous blue supergiants ($m \sim 26$) and the Tip of the Red Giant Branch (TRGB; $m \sim 31$) are effectively inaccessible in crowded, high-surface-brightness hosts. LSST will deliver exquisite SN discovery and light curves and statistical host metrics (global mass, color, SFR; local surface brightness), but resolved stellar-population work at Coma distances requires space-based (*HST* or the James Webb Space Telescope *(JWST)*) or Adaptive Optics-assisted Integral Field Unit (IFU) follow-up on 8–30 m telescopes.

To sum up, LSST will transform transient astronomy from targeted studies to population-scale astrophysics, enabling the following:

- Discovery of rare transients, transitional events bridging the existing classification scheme.
- Robust constraints on progenitor and explosion physics.
- Insights into binary evolution and mass-loss physics.
- Candidate alerts for rapid follow-up observations.

**Author Contributions:** Conceptualization, K.M.; methodology including detection and observation of SNe, all co-authors; writing—original draft preparation, all co-authors; writing—review and editing, all co-authors; supervision, K.M. All authors have read and agreed to the published version of the manuscript.

**Funding:** This research received no external funding.

**Data Availability Statement:** The data sources are cited in the manuscript.

**Acknowledgments:** We thank the reviewers for providing insightful comments, which have greatly helped to improve the manuscript. This article is based on the results published in several papers by our research group. We thank Ankur Ghosh, Dimple, Anshika Gupta, Sarvesh Kumar Yadav, Dhruv Jain, and Debalina Kar for their participation in the observing runs. Brijesh Kumar, S. B. Pandey, and Subhash Bose are duly thanked and acknowledged. We appreciate the support of the observing staff and observing assistants at the different observing facilities during the observations. We express our sincere gratitude to all our collaborators over the past decade, whose efforts have led to meaningful scientific outcomes.

**Conflicts of Interest:** The authors declare no conflicts of interest.

## Appendix A

ARIES operates modern optical observational facilities, namely the ST, DFOT, DOT and ILMT, which have been used for SN monitoring at ARIES using the Bessel and SDSS filters. A complete list of the telescopes in ARIES and the backend instruments used for SNe observations is provided in Table A1.

**Table A1.** List of ARIES telescopes and the backend instruments used for SNe observations.

| Telescope | Backend Instruments |
|---|---|
| 1.04 m Sampurnanand Telescope (ST) | **4k × 4k CCD**: *Array size*: 4096 × 4096 pixels$^2$; *FoV*: 15′.8 × 15′.8; *Gain*: 1.03, 2.15, 3.38, 5.41, and 11.05 $e^-$/ADU (at 100kHz readout speed); *Readout Noise*: 6.38, 6.71, 6.80, 7.67, and 7.84 $e^-$ (at 100kHz readout speed)<br>**1k × 1k CCD**: *Array size*: 1024 × 1024 pixel$^2$; *FoV*: 6′ × 6′; *Gain*: 11.98 $e^-$/ADU with settings of 1X, 2X, and 4X; *Readout Noise*: 7.0, 5.0 and 4.1 $e^-$<br>**Filters**: Bessel (*UBVRI*) |

**Table A1.** *Cont.*

| Telescope | Backend Instruments |
|---|---|
| 1.3 m Devasthal Fast Optical Telescope (DFOT) | **2k × 2k CCD**: *Array size*: 2048 × 2048 pixel$^2$; *FoV*: 18′ × 18′; *Gain*: 0.7, 1.4, 2.0, 2.0 e$^-$/ADU; *Readout Noise*: 2.5, 4.1, 6.5, 7.0 e$^-$<br>**iXon EM+ DU-897**: *Array size*: 512 × 512 pixel$^2$; *FoV*: 5′.5 × 5′.5; *Gain*: readout-dependent variable gain; *Readout Noise*: 1–49 e$^-$ (at 10 MHz readout speed)<br>**Filters**: Bessel (*UBVRI*) and SDSS ($u'$, $g'$, $r'$, $i'$, $z'$) |
| 3.6 m Devasthal Optical Telescope (DOT) | **IMAGER**: *Array size*: 4096 × 4096 pixel$^2$; *FoV*: 6′.5 × 6′.5; *Gain*: 1, 2, 3, 5, 10 e$^-$/ADU; *Readout noise*: 7–9 e$^-$ (at 1 MHz), 4-6 e$^-$ (at 500 kHz), 2-3 e$^-$ (at 100 kHz)<br>**Filters**: Bessel (*UBVRI)* and SDSS ($u'$, $g'$, $r'$, $i'$, $z'$)<br>**ADFOSC**: *Array size*: 4096×4096 pixel$^2$; *FoV*: 13′.6 × 13′.6; *Spectral resolution*: <2000; *wavelength range*: 350–1050 nm; *Gain*: 1.6 e$^-$/ADU; *Readout noise*: 8.0 e$^-$ **Filters**: SDSS (u, g, r, i, z) |
| 4.0 m International Liquid Mirror Telescope (ILMT) | **4k × 4k TDI mode CCD**:*Array size*: 4096 × 4096 CCD, *FoV*: 22′ × 22′; *Gain*: 4.0 e$^-$/ADU; *Readout noise*: 5.0 e$^-$<br>**Filters**: SDSS g′, r′, i′ |

## Notes

[1] https://www.wis-tns.org/ (accessed on 16 October 2025).
[2] https://aries.res.in/ (accessed on 16 October 2025).
[3] Profile is described as an absorption dip followed by an emission counterpart. The absorption part is seen due to the absorption of light in the expanding SN ejecta located at the line of sight of the observer, whereas the emission component is created due to the scattering of light from the perpendicular of the line of sight. The absorption component is blue-shifted, indicating the expansion of the SN ejecta towards the observer, whereas scattering of the light from the perpendicular side has no such effect; hence, the emission component lies at the rest wavelength of the element. In Type II SNe, this P-Cygni profile is most prominent for the H$\alpha$ line, suggesting the presence of excess hydrogen on the progenitor prior to the explosion. The absorption component of the profile measures the amount of hydrogen present.

## References

1. Filippenko, A.V. Optical Spectra of Supernovae. *Annu. Rev. Astron. Astrophys.* **1997**, *35*, 309–355. [CrossRef]
2. Minkowski, R. Spectra of Supernovae. *Publ. Astron. Soc. Pac.* **1941**, *53*, 224. [CrossRef]
3. Woosley, S.E.; Weaver, T.A. The physics of supernova explosions. *Annu. Rev. Astron. Astrophys.* **1986**, *24*, 205–253. [CrossRef]
4. Anderson, J.P.; González-Gaitán, S.; Hamuy, M.; Gutiérrez, C.P.; Stritzinger, M.D.; Olivares, F.; Phillips, M.M.; Schulze, S.; Antezana, R.; Bolt, L.; et al. Characterizing the V-band Light-curves of Hydrogen-rich Type II Supernovae. *Astrophys. J.* **2014**, *786*, 67. [CrossRef]
5. Sanders, N.E.; Soderberg, A.M.; Gezari, S.; Betancourt, M.; Chornock, R.; Berger, E.; Foley, R.J.; Challis, P.; Drout, M.; Kirshner, R.P.; et al. VizieR Online Data Catalog: Type IIP supernovae from Pan-STARRS1 (Sanders+, 2015). *Vizier Online Data Cat.* **2015**, *179*, J/ApJ/799/208.
6. Hiramatsu, D.; Howell, D.A.; Moriya, T.J.; Goldberg, J.A.; Hosseinzadeh, G.; Arcavi, I.; Anderson, J.P.; Gutiérrez, C.P.; Burke, J.; McCully, C.; et al. Luminous Type II Short-Plateau Supernovae 2006Y, 2006ai, and 2016egz: A Transitional Class from Stripped Massive Red Supergiants. *Astrophys. J.* **2021**, *913*, 55. [CrossRef]
7. Smith, N. Mass Loss: Its Effect on the Evolution and Fate of High-Mass Stars. *Annu. Rev. Astron. Astrophys.* **2014**, *52*, 487–528. [CrossRef]
8. Khazov, D.; Yaron, O.; Gal-Yam, A.; Manulis, I.; Rubin, A.; Kulkarni, S.R.; Arcavi, I.; Kasliwal, M.M.; Ofek, E.O.; Cao, Y.; et al. Flash Spectroscopy: Emission Lines from the Ionized Circumstellar Material around <10-day-old Type II Supernovae. *Astrophys. J.* **2016**, *818*, 3. [CrossRef]
9. Gangopadhyay, A.; Misra, K.; Hiramatsu, D.; Wang, S.Q.; Hosseinzadeh, G.; Wang, X.; Valenti, S.; Zhang, J.; Howell, D.A.; Arcavi, I.; et al. Flash Ionization Signatures in the Type Ibn Supernova SN 2019uo. *Astrophys. J.* **2020**, *889*, 170. [CrossRef]

10. Dukiya, N.; Gangopadhyay, A.; Misra, K.; Hosseinzadeh, G.; Bostroem, K.A.; Ailawadhi, B.; Howell, D.A.; Valenti, S.; Arcavi, I.; McCully, C.; et al. Probing the Circumstellar Environment of the Highly Luminous Type IIn Supernova ASASSN-14il. *Astrophys. J.* **2024**, *976*, 86. [CrossRef]
11. Turatto, M.; Cappellaro, E.; Danziger, I.J.; Benetti, S.; Gouiffes, C.; della Valle, M. The type II supernova 1988Z in MCG +03-28-022: Increasingevidence of interaction of supernova ejecta with a circumstellar wind. *Mon. Not. R. Astron. Soc.* **1993**, *262*, 128–140. [CrossRef]
12. Weil, K.E.; Fesen, R.A.; Patnaude, D.J.; Milisavljevic, D. Late-time Circumstellar Interaction of SN 2017eaw in NGC 6946. *Astrophys. J.* **2020**, *900*, 11. [CrossRef]
13. Rizzo Smith, M.; Kochanek, C.S.; Neustadt, J.M.M. The late time optical evolution of twelve core-collapse supernovae: Detection of normal stellar winds. *Mon. Not. R. Astron. Soc.* **2023**, *523*, 1474–1495. [CrossRef]
14. Lundqvist, P.; Fransson, C. Circumstellar Emission from SN 1987A. *Astrophys. J.* **1991**, *380*, 575. [CrossRef]
15. Jakobsen, P.; Albrecht, R.; Barbieri, C.; Blades, J.C.; Boksenberg, A.; Crane, P.; Deharveng, J.M.; Disney, M.J.; Kamperman, T.M.; King, I.R.; et al. First Results from the Faint Object Camera: SN 1987A. *Astrophys. J.* **1991**, *369*, L63. [CrossRef]
16. Branch, D.; Wheeler, J.C. *Supernova Explosions*; Springer: Berlin/Heidelberg, Germany, 2017. [CrossRef]
17. Hamuy, M.; Pinto, P.A.; Maza, J.; Suntzeff, N.B.; Phillips, M.M.; Eastman, R.G.; Smith, R.C.; Corbally, C.J.; Burstein, D.; Li, Y.; et al. The Distance to SN 1999em from the Expanding Photosphere Method. *Astrophys. J.* **2001**, *558*, 615–642. [CrossRef]
18. Terreran, G.; Jerkstrand, A.; Benetti, S.; Smartt, S.J.; Ochner, P.; Tomasella, L.; Howell, D.A.; Morales-Garoffolo, A.; Harutyunyan, A.; Kankare, E.; et al. The multifaceted Type II-L supernova 2014G from pre-maximum to nebular phase. *Mon. Not. R. Astron. Soc.* **2016**, *462*, 137–157. [CrossRef]
19. Matheson, T.; Filippenko, A.V.; Barth, A.J.; Ho, L.C.; Leonard, D.C.; Bershady, M.A.; Davis, M.; Finley, D.S.; Fisher, D.; González, R.A.; et al. Optical Spectroscopy of Supernova 1993J During Its First 2500 Days. *Astron. J.* **2000**, *120*, 1487–1498. [CrossRef]
20. Stritzinger, M.; Mazzali, P.; Phillips, M.M.; Immler, S.; Soderberg, A.; Sollerman, J.; Boldt, L.; Braithwaite, J.; Brown, P.; Burns, C.R.; et al. The He-Rich Core-Collapse Supernova 2007Y: Observations from X-Ray to Radio Wavelengths. *Astrophys. J.* **2009**, *696*, 713–728. [CrossRef]
21. Clocchiatti, A.; Wheeler, J.C.; Brotherton, M.S.; Cochran, A.L.; Wills, D.; Barker, E.S.; Turatto, M. SN 1994I: Disentangling He i Lines in Type IC Supernovae. *Astrophys. J.* **1996**, *462*, 462. [CrossRef]
22. Mazzali, P.A.; Sullivan, M.; Hachinger, S.; Ellis, R.S.; Nugent, P.E.; Howell, D.A.; Gal-Yam, A.; Maguire, K.; Cooke, J.; Thomas, R.; et al. Hubble Space Telescope spectra of the Type Ia supernova SN 2011fe: A tail of low-density, high-velocity material with $Z < Z_{\odot}$. *Mon. Not. R. Astron. Soc.* **2014**, *439*, 1959–1979. [CrossRef]
23. Smith, N.; Silverman, J.M.; Filippenko, A.V.; Cooper, M.C.; Matheson, T.; Bian, F.; Weiner, B.J.; Comerford, J.M. Systematic Blueshift of Line Profiles in the Type IIn Supernova 2010jl: Evidence for Post-shock Dust Formation? *Astron. J.* **2012**, *143*, 17. [CrossRef]
24. Pastorello, A.; Smartt, S.J.; Mattila, S.; Eldridge, J.J.; Young, D.; Itagaki, K.; Yamaoka, H.; Navasardyan, H.; Valenti, S.; Patat, F.; et al. A giant outburst two years before the core-collapse of a massive star. *Nature* **2007**, *447*, 829–832. [CrossRef] [PubMed]
25. Gal-Yam, A.; Bruch, R.; Schulze, S.; Yang, Y.; Perley, D.A.; Irani, I.; Sollerman, J.; Kool, E.C.; Soumagnac, M.T.; Yaron, O.; et al. A WC/WO star exploding within an expanding carbon-oxygen-neon nebula. *Nature* **2022**, *601*, 201–204. [CrossRef]
26. Bellm, E.C.; Kulkarni, S.R.; Barlow, T.; Feindt, U.; Graham, M.J.; Goobar, A.; Kupfer, T.; Ngeow, C.C.; Nugent, P.; Ofek, E.; et al. The Zwicky Transient Facility: Surveys and Scheduler. *Publ. Astron. Soc. Pac.* **2019**, *131*, 068003. [CrossRef]
27. Tonry, J.L.; Denneau, L.; Heinze, A.N.; Stalder, B.; Smith, K.W.; Smartt, S.J.; Stubbs, C.W.; Weiland, H.J.; Rest, A. ATLAS: A High-cadence All-sky Survey System. *Publ. Astron. Soc. Pac.* **2018**, *130*, 064505. [CrossRef]
28. Chambers, K.C.; Magnier, E.A.; Metcalfe, N.; Flewelling, H.A.; Huber, M.E.; Waters, C.Z.; Denneau, L.; Draper, P.W.; Farrow, D.; Finkbeiner, D.P.; et al. The Pan-STARRS1 Surveys. *arXiv* **2016**, arXiv:1612.05560. [CrossRef]
29. Shappee, B.; Prieto, J.; Stanek, K.Z.; Kochanek, C.S.; Holoien, T.; Jencson, J.; Basu, U.; Beacom, J.F.; Szczygiel, D.; Pojmanski, G.; et al. All Sky Automated Survey for SuperNovae (ASAS-SN or "Assassin"). In Proceedings of the American Astronomical Society Meeting Abstracts #223, Washington, DC, USA, 5–9 January 2014; Volume 223, p. 236.03.
30. Surdej, J.; Hickson, P.; Misra, K.; Banerjee, D.; Ailawadhi, B.; Akhunov, T.; Borra, E.; Dubey, M.; Dukiya, N.; Filali, S.; et al. The 4 m International Liquid Mirror Telescope: Construction, operation, and science. *Astron. Astrophys.* **2025**, *694*, A80. [CrossRef]
31. Tartaglia, L.; Sand, D.J.; Valenti, S.; Wyatt, S.; Anderson, J.P.; Arcavi, I.; Ashall, C.; Botticella, M.T.; Cartier, R.; Chen, T.W.; et al. The Early Detection and Follow-up of the Highly Obscured Type II Supernova 2016ija/DLT16am. *Astrophys. J.* **2018**, *853*, 62. [CrossRef]
32. Sinvhal, S.D.; Kandpal, C.D.; Mahra, H.S.; Joshi, S.C.; Srivastava, J.B. The 104-cm telescope of Uttar Pradesh State Observatory. In Proceedings of the Optical Astronomy with Moderate Size Telescopes, Tucson, AZ, USA, 1–3 February 1972; pp. 20–34.
33. Joshi, Y.C.; Bangia, T.; Jaiswar, M.K.; Pant, J.; Reddy, K.; Yadav, S. ARIES 130-cm Devasthal Fast Optical Telescope—Operation and Outcome. *J. Astron. Instrum.* **2022**, *11*, 2240004. [CrossRef]

34. Kumar, B.; Omar, A.; Maheswar, G.; Pandey, A.K.; Sagar, R.; Uddin, W.; Sanwal, B.B.; Bangia, T.; Kumar, T.S.; Yadav, S.; et al. 3.6-m Devasthal Optical Telescope Project: Completion and first results. *Bull. Soc. R. Sci. Liege* **2018**, *87*, 29–41.
35. Pandey, S.B.; Yadav, R.K.S.; Nanjappa, N.; Yadav, S.; Reddy, B.K.; Sahu, S.; Srinivasan, R. First-light instrument for the 3.6-m Devasthal Optical Telescope: 4Kx4K CCD Imager. *Bull. Soc. R. Sci. Liege* **2018**, *87*, 42–57. [CrossRef]
36. Omar, A.; Kumar, T.S.; Krishna Reddy, B.; Pant, J.; Mahto, M. First-Light Images from Low-Dispersion Spectrograph-Cum-Imager on 3.6 m Devasthal Optical Telescope. *Curr. Sci.* **2019**, *116*, 1472. [CrossRef]
37. Prabhu, T.P.; Anupama, G.C. Science with Indian Astronomical Observatory, Hanle. In Proceedings of the Astronomical Society of India Conference Series, Pune, India, 14–17 February 2010; Astronomical Society of India Conference Series; Volume 1.
38. Brown, T.M.; Baliber, N.; Bianco, F.B.; Bowman, M.; Burleson, B.; Conway, P.; Crellin, M.; Depagne, É.; De Vera, J.; Dilday, B.; et al. Las Cumbres Observatory Global Telescope Network. *Publ. Astron. Soc. Pac.* **2013**, *125*, 1031. [CrossRef]
39. Pranshu, K.; Misra, K.; Ailawadhi, B.; Dubey, M.; Dukiya, N.; Filali, S.; Hickson, P.; Kumar, B.; Negi, V.; Surdej, J. PYLMT: A transient detection pipeline for the 4-m International Liquid Mirror Telescope. *Mon. Not. R. Astron. Soc.* **2025**, *538*, 133–152. [CrossRef]
40. Richardson, D.; Branch, D.; Casebeer, D.; Millard, J.; Thomas, R.C.; Baron, E. A Comparative Study of the Absolute Magnitude Distributions of Supernovae. *Astron. J.* **2002**, *123*, 745–752. [CrossRef]
41. Phillips, M.M. The absolute magnitudes of Type IA supernovae. *Astrophys. J.* **1993**, *413*, L105–L108. [CrossRef]
42. Phillips, M.M.; Lira, P.; Suntzeff, N.B.; Schommer, R.A.; Hamuy, M.; Maza, J. The Reddening-Free Decline Rate Versus Luminosity Relationship for Type IA Supernovae. *Astron. J.* **1999**, *118*, 1766–1776. [CrossRef]
43. Filippenko, A.V.; Richmond, M.W.; Branch, D.; Gaskell, C.M.; Herbst, W.; Ford, C.H.; Treffers, R.R.; Matheson, T.; Ho, L.C.; Dey, A.; et al. The peculiar Type IA supernova 1991T: Detonation of a white dwarf? *Astron. J.* **1992**, *103*, 1632–1646. [CrossRef]
44. Filippenko, A.V.; Richmond, M.W.; Branch, D.; Gaskell, M.; Herbst, W.; Ford, C.H.; Treffers, R.R.; Matheson, T.; Ho, L.C.; Dey, A.; et al. The subluminous, spectroscopically peculiar type IA supernova 1991bg in the elliptical galaxy NGC 4374. *Astron. J.* **1992**, *104*, 1543–1556. [CrossRef]
45. Foley, R.J.; Challis, P.J.; Chornock, R.; Ganeshalingam, M.; Li, W.; Marion, G.H.; Morrell, N.I.; Pignata, G.; Stritzinger, M.D.; Silverman, J.M.; et al. Type Iax Supernovae: A New Class of Stellar Explosion. *Astrophys. J.* **2013**, *767*, 57. [CrossRef]
46. Jha, S.W. Type Iax Supernovae. In *Handbook of Supernovae*; Alsabti, A.W., Murdin, P., Eds.; Springer: Cham, Switzerland, 2017; p. 375. [CrossRef]
47. Li, W.; Filippenko, A.V.; Chornock, R.; Berger, E.; Berlind, P.; Calkins, M.L.; Challis, P.; Fassnacht, C.; Jha, S.; Kirshner, R.P.; et al. SN 2002cx: The Most Peculiar Known Type Ia Supernova. *Publ. Astron. Soc. Pac.* **2003**, *115*, 453–473. [CrossRef]
48. Karambelkar, V.R.; Kasliwal, M.M.; Maguire, K.; Anand, S.G.; Andreoni, I.; De, K.; Drake, A.; Duev, D.A.; Graham, M.J.; Kool, E.C.; et al. Faintest of Them All: ZTF 21aaoryiz/SN 2021fcg—Discovery of an Extremely Low Luminosity Type Iax Supernova. *Astrophys. J. Lett.* **2021**, *921*, L6. [CrossRef]
49. Stritzinger, M.D.; Valenti, S.; Hoeflich, P.; Baron, E.; Phillips, M.M.; Taddia, F.; Foley, R.J.; Hsiao, E.Y.; Jha, S.W.; McCully, C.; et al. Comprehensive observations of the bright and energetic Type Iax SN 2012Z: Interpretation as a Chandrasekhar mass white dwarf explosion. *Astron. Astrophys.* **2015**, *573*, A2. [CrossRef]
50. Magee, M.R.; Kotak, R.; Sim, S.A.; Kromer, M.; Rabinowitz, D.; Smartt, S.J.; Baltay, C.; Campbell, H.C.; Chen, T.W.; Fink, M.; et al. The type Iax supernova, SN 2015H. A white dwarf deflagration candidate. *Astron. Astrophys.* **2016**, *589*, A89. [CrossRef]
51. Magee, M.R.; Kotak, R.; Sim, S.A.; Wright, D.; Smartt, S.J.; Berger, E.; Chornock, R.; Foley, R.J.; Howell, D.A.; Kaiser, N.; et al. Growing evidence that SNe Iax are not a one-parameter family. The case of PS1-12bwh. *Astron. Astrophys.* **2017**, *601*, A62. [CrossRef]
52. Li, L.; Wang, X.; Zhang, J.; Arcavi, I.; Zhang, T.; Rui, L.; Hosseinzadeh, G.; Howell, D.A.; McCully, C.; Zhang, K.; et al. Optical observations of the 2002cx-like supernova 2014ek and characterizations of SNe Iax. *Mon. Not. R. Astron. Soc.* **2018**, *478*, 4575–4589. [CrossRef]
53. Taubenberger, S. The Extremes of Thermonuclear Supernovae. In *Handbook of Supernovae*; Alsabti, A.W., Murdin, P., Eds.; Springer: Berlin/Heidelberg, Germany, 2017; p. 317. [CrossRef]
54. Foley, R.J.; Chornock, R.; Filippenko, A.V.; Ganeshalingam, M.; Kirshner, R.P.; Li, W.; Cenko, S.B.; Challis, P.J.; Friedman, A.S.; Modjaz, M.; et al. SN 2008ha: An Extremely Low Luminosity and Exceptionally Low Energy Supernova. *Astron. J.* **2009**, *138*, 376–391. [CrossRef]
55. Maguire, K.; Magee, M.R.; Leloudas, G.; Miller, A.A.; Dimitriadis, G.; Pursiainen, M.; Bulla, M.; De, K.; Gal-Yam, A.; Perley, D.A.; et al. SN 2020udy: An SN Iax with strict limits on interaction consistent with a helium-star companion. *Mon. Not. R. Astron. Soc.* **2023**, *525*, 1210–1228. [CrossRef]
56. Camacho-Neves, Y.; Jha, S.W.; Barna, B.; Dai, M.; Filippenko, A.V.; Foley, R.J.; Hosseinzadeh, G.; Howell, D.A.; Johansson, J.; Kelly, P.L.; et al. Over 500 Days in the Life of the Photosphere of the Type Iax Supernova SN 2014dt. *Astrophys. J.* **2023**, *951*, 67. [CrossRef]

57. Foley, R.J.; Jha, S.W.; Pan, Y.C.; Zheng, W.K.; Bildsten, L.; Filippenko, A.V.; Kasen, D. Late-time spectroscopy of Type Iax Supernovae. *Mon. Not. R. Astron. Soc.* **2016**, *461*, 433–457. [CrossRef]
58. Singh, M.; Misra, K.; Sahu, D.K.; Dastidar, R.; Gangopadhyay, A.; Bose, S.; Srivastav, S.; Anupama, G.C.; Chakradhari, N.K.; Kumar, B.; et al. Exploring the optical behaviour of a Type Iax supernova SN 2014dt. *Mon. Not. R. Astron. Soc.* **2018**, *474*, 2551–2563. [CrossRef]
59. Foley, R.J.; Van Dyk, S.D.; Jha, S.W.; Clubb, K.I.; Filippenko, A.V.; Mauerhan, J.C.; Miller, A.A.; Smith, N. On the Progenitor System of the Type Iax Supernova 2014dt in M61. *Astrophys. J.* **2015**, *798*, L37. [CrossRef]
60. Fox, O.D.; Johansson, J.; Kasliwal, M.; Andrews, J.; Bally, J.; Bond, H.E.; Boyer, M.L.; Gehrz, R.D.; Helou, G.; Hsiao, E.Y.; et al. An Excess of Mid-infrared Emission from the Type Iax SN 2014dt. *Astrophys. J.* **2016**, *816*, L13. [CrossRef]
61. McClelland, C.M.; Garnavich, P.M.; Galbany, L.; Miquel, R.; Foley, R.J.; Filippenko, A.V.; Bassett, B.; Wheeler, J.C.; Goobar, A.; Jha, S.W.; et al. The Subluminous Supernova 2007qd: A Missing Link in a Family of Low-luminosity Type Ia Supernovae. *Astrophys. J.* **2010**, *720*, 704–716. [CrossRef]
62. Narayan, G.; Foley, R.J.; Berger, E.; Botticella, M.T.; Chornock, R.; Huber, M.E.; Rest, A.; Scolnic, D.; Smartt, S.; Valenti, S.; et al. Displaying the Heterogeneity of the SN 2002cx-like Subclass of Type Ia Supernovae with Observations of the Pan-STARRS-1 Discovered SN 2009ku. *Astrophys. J.* **2011**, *731*, L11. [CrossRef]
63. Tomasella, L.; Cappellaro, E.; Benetti, S.; Pastorello, A.; Hsiao, E.Y.; Sand, D.J.; Stritzinger, M.; Valenti, S.; McCully, C.; Arcavi, I.; et al. Optical and near-infrared observations of SN 2014ck: An outlier among the Type Iax supernovae. *Mon. Not. R. Astron. Soc.* **2016**, *459*, 1018–1038. [CrossRef]
64. Singh, M.; Sahu, D.K.; Dastidar, R.; Barna, B.; Misra, K.; Gangopadhyay, A.; Howell, D.A.; Jha, S.W.; Im, H.; Taggart, K.; et al. Observational Properties of a Bright Type lax SN 2018cni and a Faint Type Iax SN 2020kyg. *Astrophys. J.* **2023**, *953*, 93. [CrossRef]
65. Dutta, A.; Sahu, D.K.; Anupama, G.C.; Joharle, S.; Kumar, B.; Nayana, A.J.; Singh, A.; Kumar, H.; Bhalerao, V.; Barway, S. SN 2020sck: Deflagration in a Carbon-Oxygen White Dwarf. *Astrophys. J.* **2022**, *925*, 217. [CrossRef]
66. Singh, M.; Misra, K.; Sahu, D.K.; Ailawadhi, B.; Dutta, A.; Howell, D.A.; Anupama, G.C.; Bostroem, K.A.; Burke, J.; Dastidar, R.; et al. Optical studies of a bright Type Iax supernova SN 2020rea. *Mon. Not. R. Astron. Soc.* **2022**, *517*, 5617–5626. [CrossRef]
67. Singh, M.; Sahu, D.K.; Barna, B.; Gangopadhyay, A.; Dastidar, R.; Teja, R.S.; Misra, K.; Howell, D.A.; Wang, X.; Mo, J.; et al. SN 2020udy: A New Piece of the Homogeneous Bright Group in the Diverse Iax Subclass. *Astrophys. J.* **2024**, *965*, 73. [CrossRef]
68. Fink, M.; Kromer, M.; Seitenzahl, I.R.; Ciaraldi-Schoolmann, F.; Röpke, F.K.; Sim, S.A.; Pakmor, R.; Ruiter, A.J.; Hillebrandt, W. Three-dimensional pure deflagration models with nucleosynthesis and synthetic observables for Type Ia supernovae. *Mon. Not. R. Astron. Soc.* **2014**, *438*, 1762–1783. [CrossRef]
69. Fernández, R.; Metzger, B.D. Nuclear Dominated Accretion Flows In Two Dimensions. I. Torus Evolution With Parametric Microphysics. *Astrophys. J.* **2013**, *763*, 108. [CrossRef]
70. Kashyap, R.; Haque, T.; Lorén-Aguilar, P.; García-Berro, E.; Fisher, R. Double-degenerate Carbon-Oxygen and Oxygen-Neon White Dwarf Mergers: A New Mechanism for Faint and Rapid Type Ia Supernovae. *Astrophys. J.* **2018**, *869*, 140. [CrossRef] [PubMed]
71. Denissenkov, P.A.; Truran, J.W.; Herwig, F.; Jones, S.; Paxton, B.; Nomoto, K.; Suzuki, T.; Toki, H. Hybrid C-O-Ne white dwarfs as progenitors of Type Ia supernovae: Dependence on Urca process and mixing assumptions. *Mon. Not. R. Astron. Soc.* **2015**, *447*, 2696–2705. [CrossRef]
72. Kromer, M.; Ohlmann, S.T.; Pakmor, R.; Ruiter, A.J.; Hillebrandt, W.; Marquardt, K.S.; Röpke, F.K.; Seitenzahl, I.R.; Sim, S.A.; Taubenberger, S. Deflagrations in hybrid CONe white dwarfs: A route to explain the faint Type Iax supernova 2008ha . *Mon. Not. R. Astron. Soc.* **2015**, *450*, 3045–3053. [CrossRef]
73. Bravo, E.; Gil-Pons, P.; Gutiérrez, J.L.; Doherty, C.L. Explosion of white dwarfs harboring hybrid CONe cores. *Astron. Astrophys.* **2016**, *589*, A38. [CrossRef]
74. Lach, F.; Callan, F.P.; Bubeck, D.; Röpke, F.K.; Sim, S.A.; Schrauth, M.; Ohlmann, S.T.; Kromer, M. Type Iax supernovae from deflagrations in Chandrasekhar mass white dwarfs. *Astron. Astrophys.* **2022**, *658*, A179. [CrossRef]
75. Moriya, T.; Tominaga, N.; Tanaka, M.; Nomoto, K.; Sauer, D.N.; Mazzali, P.A.; Maeda, K.; Suzuki, T. Fallback Supernovae: A Possible Origin of Peculiar Supernovae with Extremely Low Explosion Energies. *Astrophys. J.* **2010**, *719*, 1445–1453. [CrossRef]
76. Bobrick, A.; Zenati, Y.; Perets, H.B.; Davies, M.B.; Church, R. Transients from ONe white dwarf—Neutron star/black hole mergers. *Mon. Not. R. Astron. Soc.* **2022**, *510*, 3758–3777. [CrossRef]
77. Pumo, M.L.; Turatto, M.; Botticella, M.T.; Pastorello, A.; Valenti, S.; Zampieri, L.; Benetti, S.; Cappellaro, E.; Patat, F. EC-SNe From Super-Asymptotic Giant Branch Progenitors: Theoretical Models Versus Observations. *Astrophys. J.* **2009**, *705*, L138–L142. [CrossRef]
78. Barna, B.; Szalai, T.; Jha, S.W.; Camacho-Neves, Y.; Kwok, L.; Foley, R.J.; Kilpatrick, C.D.; Coulter, D.A.; Dimitriadis, G.; Rest, A.; et al. SN 2019muj—A well-observed Type Iax supernova that bridges the luminosity gap of the class. *Mon. Not. R. Astron. Soc.* **2021**, *501*, 1078–1099. [CrossRef]

79. Singh, M.; Kwok, L.A.; Jha, S.W.; Dastidar, R.; Larison, C.; Filippenko, A.V.; Andrews, J.E.; Andrews, M.; Anupama, G.C.; Arunachalam, P.; et al. Photometry and Spectroscopy of SN 2024pxl: A Luminosity Link Among Type Iax Supernovae. *arXiv* **2025**, arXiv:2505.02943. [CrossRef]
80. Magee, M.R.; Killestein, T.L.; Pursiainen, M.; Godson, B.; Jarvis, D.; Jiménez-Palau, C.; Lyman, J.D.; Steeghs, D.; Warwick, B.; Anderson, J.P.; et al. SN 2024bfu, SN 2025qe, and the early light curves of type Iax supernovae. *arXiv* **2025**, arXiv:2506.02118. [CrossRef]
81. Barbon, R.; Ciatti, F.; Rosino, L. Photometric properties of type II supernovae. *Astron. Astrophys.* **1979**, *72*, 287–292.
82. Li, W.; Leaman, J.; Chornock, R.; Filippenko, A.V.; Poznanski, D.; Ganeshalingam, M.; Wang, X.; Modjaz, M.; Jha, S.; Foley, R.J.; et al. Nearby supernova rates from the Lick Observatory Supernova Search—II. The observed luminosity functions and fractions of supernovae in a complete sample. *Mon. Not. R. Astron. Soc.* **2011**, *412*, 1441–1472. [CrossRef]
83. Graur, O.; Bianco, F.B.; Modjaz, M. A unified explanation for the supernova rate-galaxy mass dependence based on supernovae detected in Sloan galaxy spectra. *Mon. Not. R. Astron. Soc.* **2015**, *450*, 905–925. [CrossRef]
84. Smartt, S.J.; Eldridge, J.J.; Crockett, R.M.; Maund, J.R. The death of massive stars—I. Observational constraints on the progenitors of Type II-P supernovae. *Mon. Not. R. Astron. Soc.* **2009**, *395*, 1409–1437. [CrossRef]
85. Van Dyk, S.D.; Cenko, S.B.; Poznanski, D.; Arcavi, I.; Gal-Yam, A.; Filippenko, A.V.; Silverio, K.; Stockton, A.; Cuillandre, J.C.; Marcy, G.W.; et al. The Red Supergiant Progenitor of Supernova 2012aw (PTF12bvh) in Messier 95. *Astrophys. J.* **2012**, *756*, 131. [CrossRef]
86. Van Dyk, S.D.; Davidge, T.J.; Elias-Rosa, N.; Taubenberger, S.; Li, W.; Levesque, E.M.; Howerton, S.; Pignata, G.; Morrell, N.; Hamuy, M.; et al. Supernova 2008bk and Its Red Supergiant Progenitor. *Astron. J.* **2012**, *143*, 19. [CrossRef]
87. Smartt, S.J. Observational Constraints on the Progenitors of Core-Collapse Supernovae: The Case for Missing High-Mass Stars. *Publ. Astron. Soc. Aust.* **2015**, *32*, e016. [CrossRef]
88. Woosley, S.E.; Heger, A.; Weaver, T.A. The evolution and explosion of massive stars. *Rev. Mod. Phys.* **2002**, *74*, 1015–1071. [CrossRef]
89. Heger, A.; Fryer, C.L.; Woosley, S.E.; Langer, N.; Hartmann, D.H. How Massive Single Stars End Their Life. *Astrophys. J.* **2003**, *591*, 288–300. [CrossRef]
90. Swartz, D.A.; Wheeler, J.C.; Harkness, R.P. Model Light Curves of Linear Type II Supernovae. *Astrophys. J.* **1991**, *374*, 266. [CrossRef]
91. Blinnikov, S.I.; Bartunov, O.S. Non-equilibrium radiative transfer in supernova theory: Models of linear type II supernovae. *Astron. Astrophys.* **1993**, *273*, 106–122.
92. Popov, D.V. An Analytical Model for the Plateau Stage of Type II Supernovae. *Astrophys. J.* **1993**, *414*, 712. [CrossRef]
93. Morozova, V.; Piro, A.L.; Valenti, S. Unifying Type II Supernova Light Curves with Dense Circumstellar Material. *Astrophys. J.* **2017**, *838*, 28. [CrossRef]
94. Hillier, D.J.; Dessart, L. Photometric and spectroscopic diversity of Type II supernovae. *Astron. Astrophys.* **2019**, *631*, A8. [CrossRef]
95. Singh, A.; Srivastav, S.; Kumar, B.; Anupama, G.C.; Sahu, D.K. ASASSN-14dq: A fast-declining Type II-P supernova in a low-luminosity host galaxy. *Mon. Not. R. Astron. Soc.* **2018**, *480*, 2475–2500. [CrossRef]
96. Valenti, S.; Howell, D.A.; Stritzinger, M.D.; Graham, M.L.; Hosseinzadeh, G.; Arcavi, I.; Bildsten, L.; Jerkstrand, A.; McCully, C.; Pastorello, A.; et al. The diversity of Type II supernova versus the similarity in their progenitors. *Mon. Not. R. Astron. Soc.* **2016**, *459*, 3939–3962. [CrossRef]
97. Anderson, J.P. A meta-analysis of core-collapse supernova $^{56}$Ni masses. *Astron. Astrophys.* **2019**, *628*, A7. [CrossRef]
98. Kasen, D.; Woosley, S.E. Type II Supernovae: Model Light Curves and Standard Candle Relationships. *Astrophys. J.* **2009**, *703*, 2205–2216. [CrossRef]
99. Ailawadhi, B.; Dastidar, R.; Misra, K.; Roy, R.; Hiramatsu, D.; Howell, D.A.; Brink, T.G.; Zheng, W.; Galbany, L.; Shahbandeh, M.; et al. Photometric and spectroscopic analysis of the Type II SN 2020jfo with a short plateau. *Mon. Not. R. Astron. Soc.* **2023**, *519*, 248–270. [CrossRef]
100. Dastidar, R.; Misra, K.; Singh, M.; Pastorello, A.; Sahu, D.K.; Wang, X.; Gangopadhyay, A.; Tomasella, L.; Zhang, J.; Bose, S.; et al. The optical properties of three Type II supernovae: 2014cx, 2014cy, and 2015cz. *Mon. Not. R. Astron. Soc.* **2021**, *504*, 1009–1028. [CrossRef]
101. Dastidar, R.; Misra, K.; Valenti, S.; Burke, J.; Hosseinzadeh, G.; Gangopadhyay, A.; Howell, D.A.; Singh, M.; Arcavi, I.; Kumar, B.; et al. SN 2015an: A normal luminosity type II supernova with low expansion velocity at early phases. *Mon. Not. R. Astron. Soc.* **2019**, *490*, 1605–1619. [CrossRef]
102. Dastidar, R.; Misra, K.; Hosseinzadeh, G.; Pastorello, A.; Pumo, M.L.; Valenti, S.; McCully, C.; Tomasella, L.; Arcavi, I.; Elias-Rosa, N.; et al. SN 2015ba: A Type IIP supernova with a long plateau. *Mon. Not. R. Astron. Soc.* **2018**, *479*, 2421–2442. [CrossRef]
103. Dastidar, R.; Misra, K.; Singh, M.; Sahu, D.K.; Pastorello, A.; Gangopadhyay, A.; Tomasella, L.; Benetti, S.; Terreran, G.; Sanwal, P.; et al. SN 2016B a.k.a. ASASSN-16ab: A transitional Type II supernova. *Mon. Not. R. Astron. Soc.* **2019**, *486*, 2850–2872. [CrossRef]

104. Osterbrock, D.E.; Ferland, G.J. *Astrophysics of Gaseous Nebulae and Active Galactic Nuclei*; University Science Books: Dulles, VA, USA, 2006.
105. Yaron, O.; Perley, D.A.; Gal-Yam, A.; Groh, J.H.; Horesh, A.; Ofek, E.O.; Kulkarni, S.R.; Sollerman, J.; Fransson, C.; Rubin, A.; et al. Confined dense circumstellar material surrounding a regular type II supernova. *Nat. Phys.* **2017**, *13*, 510–517. [CrossRef]
106. Bostroem, K.A.; Pearson, J.; Shrestha, M.; Sand, D.J.; Valenti, S.; Jha, S.W.; Andrews, J.E.; Smith, N.; Terreran, G.; Green, E.; et al. Early Spectroscopy and Dense Circumstellar Medium Interaction in SN 2023ixf. *Astrophys. J.* **2023**, *956*, L5. [CrossRef]
107. Dessart, L.; Jacobson-Galán, W.V. Using spectral modeling to break light-curve degeneracies of type II supernovae interacting with circumstellar material. *Astron. Astrophys.* **2023**, *677*, A105. [CrossRef]
108. Niemela, V.S.; Ruiz, M.T.; Phillips, M.M. The supernova 1983k in NGC 4699: Clues to the nature of type II progenitors. *Astrophys. J.* **1985**, *289*, 52–57. [CrossRef]
109. Benetti, S.; Cappellaro, E.; Turatto, M.; della Valle, M.; Mazzali, P.A.; Gouiffes, C. The late evolution of the type II SN 1990E. *Astron. Astrophys.* **1994**, *285*, 147–156.
110. Leonard, D.C.; Filippenko, A.V.; Barth, A.J.; Matheson, T. Evidence for Asphericity in the Type IIN Supernova SN 1998S. *Astrophys. J.* **2000**, *536*, 239–254. [CrossRef]
111. Smith, N.; Mauerhan, J.C.; Cenko, S.B.; Kasliwal, M.M.; Silverman, J.M.; Filippenko, A.V.; Gal-Yam, A.; Clubb, K.I.; Graham, M.L.; Leonard, D.C.; et al. PTF11iqb: Cool supergiant mass-loss that bridges the gap between Type IIn and normal supernovae. *Mon. Not. R. Astron. Soc.* **2015**, *449*, 1876–1896. [CrossRef]
112. Hosseinzadeh, G.; Valenti, S.; McCully, C.; Howell, D.A.; Arcavi, I.; Jerkstrand, A.; Guevel, D.; Tartaglia, L.; Rui, L.; Mo, J.; et al. Short-lived Circumstellar Interaction in the Low-luminosity Type IIP SN 2016bkv. *Astrophys. J.* **2018**, *861*, 63. [CrossRef]
113. Bruch, R.J.; Gal-Yam, A.; Yaron, O.; Chen, P.; Strotjohann, N.L.; Irani, I.; Zimmerman, E.; Schulze, S.; Yang, Y.; Kim, Y.L.; et al. The Prevalence and Influence of Circumstellar Material around Hydrogen-rich Supernova Progenitors. *Astrophys. J.* **2023**, *952*, 119. [CrossRef]
114. Groh, J.H. Early-time spectra of supernovae and their precursor winds. The luminous blue variable/yellow hypergiant progenitor of SN 2013cu. *Astron. Astrophys.* **2014**, *572*, L11. [CrossRef]
115. Shivvers, I.; Groh, J.H.; Mauerhan, J.C.; Fox, O.D.; Leonard, D.C.; Filippenko, A.V. Early Emission from the Type IIn Supernova 1998S at High Resolution. *Astrophys. J.* **2015**, *806*, 213. [CrossRef]
116. Bullivant, C.; Smith, N.; Williams, G.G.; Mauerhan, J.C.; Andrews, J.E.; Fong, W.F.; Bilinski, C.; Kilpatrick, C.D.; Milne, P.A.; Fox, O.D.; et al. SN 2013fs and SN 2013fr: Exploring the circumstellar-material diversity in Type II supernovae. *Mon. Not. R. Astron. Soc.* **2018**, *476*, 1497–1518. [CrossRef]
117. Pearson, J.; Hosseinzadeh, G.; Sand, D.J.; Andrews, J.E.; Jencson, J.E.; Dong, Y.; Bostroem, K.A.; Valenti, S.; Janzen, D.; Retamal, N.M.; et al. Circumstellar Medium Interaction in SN 2018lab, A Low-luminosity Type IIP Supernova Observed with TESS. *Astrophys. J.* **2023**, *945*, 107. [CrossRef]
118. Hosseinzadeh, G.; Kilpatrick, C.D.; Dong, Y.; Sand, D.J.; Andrews, J.E.; Bostroem, K.A.; Janzen, D.; Jencson, J.E.; Lundquist, M.; Meza Retamal, N.E.; et al. Weak Mass Loss from the Red Supergiant Progenitor of the Type II SN 2021yja. *Astrophys. J.* **2022**, *935*, 31. [CrossRef]
119. Qin, Y.J.; Zhang, K.; Bloom, J.; Sollerman, J.; Zimmerman, E.A.; Irani, I.; Schulze, S.; Gal-Yam, A.; Kasliwal, M.; Coughlin, M.W.; et al. The progenitor star of SN 2023ixf: A massive red supergiant with enhanced, episodic pre-supernova mass loss. *Mon. Not. R. Astron. Soc.* **2024**, *534*, 271–280. [CrossRef]
120. Jacobson-Galán, W.V.; Davis, K.W.; Kilpatrick, C.D.; Dessart, L.; Margutti, R.; Chornock, R.; Foley, R.J.; Arunachalam, P.; Auchettl, K.; Bom, C.R.; et al. SN 2024ggi in NGC 3621: Rising Ionization in a Nearby, Circumstellar-material-interacting Type II Supernova. *Astrophys. J.* **2024**, *972*, 177. [CrossRef]
121. Gutiérrez, C.P.; Anderson, J.P.; Hamuy, M.; González-Gaitan, S.; Galbany, L.; Dessart, L.; Stritzinger, M.D.; Phillips, M.M.; Morrell, N.; Folatelli, G. Type II Supernova Spectral Diversity. II. Spectroscopic and Photometric Correlations. *Astrophys. J.* **2017**, *850*, 90. [CrossRef]
122. Baron, E.; Branch, D.; Hauschildt, P.H.; Filippenko, A.V.; Kirshner, R.P.; Challis, P.M.; Jha, S.; Chevalier, R.; Fransson, C.; Lundqvist, P.; et al. Preliminary Spectral Analysis of the Type II Supernova 1999EM. *Astrophys. J.* **2000**, *545*, 444–448. [CrossRef]
123. Pastorello, A.; Sauer, D.; Taubenberger, S.; Mazzali, P.A.; Nomoto, K.; Kawabata, K.S.; Benetti, S.; Elias-Rosa, N.; Harutyunyan, A.; Navasardyan, H.; et al. SN 2005cs in M51—I. The first month of evolution of a subluminous SN II plateau. *Mon. Not. R. Astron. Soc.* **2006**, *370*, 1752–1762. [CrossRef]
124. Inserra, C.; Turatto, M.; Pastorello, A.; Benetti, S.; Cappellaro, E.; Pumo, M.L.; Zampieri, L.; Agnoletto, I.; Bufano, F.; Botticella, M.T.; et al. The Type IIP SN 2007od in UGC 12846: From a bright maximum to dust formation in the nebular phase. *Mon. Not. R. Astron. Soc.* **2011**, *417*, 261–279. [CrossRef]
125. Gutiérrez, C.P.; Anderson, J.P.; Hamuy, M.; Morrell, N.; González-Gaitan, S.; Stritzinger, M.D.; Phillips, M.M.; Galbany, L.; Folatelli, G.; Dessart, L.; et al. Type II Supernova Spectral Diversity. I. Observations, Sample Characterization, and Spectral Line Evolution. *Astrophys. J.* **2017**, *850*, 89. [CrossRef]

126. Pooley, D.; Lewin, W.H.G.; Fox, D.W.; Miller, J.M.; Lacey, C.K.; Van Dyk, S.D.; Weiler, K.W.; Sramek, R.A.; Filippenko, A.V.; Leonard, D.C.; et al. X-Ray, Optical, and Radio Observations of the Type II Supernovae 1999em and 1998S. *Astrophys. J.* **2002**, *572*, 932–943. [CrossRef]
127. Chugai, N.N.; Chevalier, R.A.; Utrobin, V.P. Optical Signatures of Circumstellar Interaction in Type IIP Supernovae. *Astrophys. J.* **2007**, *662*, 1136–1147. [CrossRef]
128. Woosley, S.E.; Weaver, T.A. The Evolution and Explosion of Massive Stars. II. Explosive Hydrodynamics and Nucleosynthesis. *Astrophys. J.* **1995**, *101*, 181. [CrossRef]
129. Jerkstrand, A.; Fransson, C.; Maguire, K.; Smartt, S.; Ergon, M.; Spyromilio, J. The progenitor mass of the Type IIP supernova SN 2004et from late-time spectral modeling. *Astron. Astrophys.* **2012**, *546*, A28. [CrossRef]
130. Jerkstrand, A.; Smartt, S.J.; Fraser, M.; Fransson, C.; Sollerman, J.; Taddia, F.; Kotak, R. The nebular spectra of SN 2012aw and constraints on stellar nucleosynthesis from oxygen emission lines. *Mon. Not. R. Astron. Soc.* **2014**, *439*, 3694–3703. [CrossRef]
131. Patat, F.; Barbon, R.; Cappellaro, E.; Turatto, M. Light curves of type II supernovae. I. The atlas. *Astron. Astrophys.* **1993**, *98*, 443–476.
132. Faran, T.; Poznanski, D.; Filippenko, A.V.; Chornock, R.; Foley, R.J.; Ganeshalingam, M.; Leonard, D.C.; Li, W.; Modjaz, M.; Serduke, F.J.D.; et al. A sample of Type II-L supernovae. *Mon. Not. R. Astron. Soc.* **2014**, *445*, 554–569. [CrossRef]
133. de Jaeger, T.; Zheng, W.; Stahl, B.E.; Filippenko, A.V.; Brink, T.G.; Bigley, A.; Blanchard, K.; Blanchard, P.K.; Bradley, J.; Cargill, S.K.; et al. The Berkeley sample of Type II supernovae: BVRI light curves and spectroscopy of 55 SNe II. *Mon. Not. R. Astron. Soc.* **2019**, *490*, 2799–2821. [CrossRef]
134. Patat, F.; Barbon, R.; Cappellaro, E.; Turatto, M. Light curves of type II supernovae. II. The analysis. *Astron. Astrophys.* **1994**, *282*, 731–741.
135. Gutiérrez, C.P.; Anderson, J.P.; Hamuy, M.; González-Gaitán, S.; Folatelli, G.; Morrell, N.I.; Stritzinger, M.D.; Phillips, M.M.; McCarthy, P.; Suntzeff, N.B.; et al. $H_\alpha$ Spectral Diversity of Type II Supernovae: Correlations with Photometric Properties. *Astrophys. J.* **2014**, *786*, L15. [CrossRef]
136. Grassberg, E.K.; Imshennik, V.S.; Nadyozhin, D.K. On the Theory of the Light Curves of Supernovae. *Astrophys. Space Sci.* **1971**, *10*, 28–51. [CrossRef]
137. Falk, S.W.; Arnett, W.D. Radiation Dynamics, Envelope Ejection, and Supernova Light Curves. *Astrophys. J.* **1977**, *33*, 515. [CrossRef]
138. Arnett, W.D. Analytic solutions for light curves of supernovae of Type II. *Astrophys. J.* **1980**, *237*, 541–549. [CrossRef]
139. Eldridge, J.J.; Tout, C.A. The progenitors of core-collapse supernovae. *Mon. Not. R. Astron. Soc.* **2004**, *353*, 87–97. [CrossRef]
140. Van Dyk, S.D.; Li, W.; Filippenko, A.V. On the Progenitor of the Type II-Plateau Supernova 2003gd in M74. *Publ. Astron. Soc. Pac.* **2003**, *115*, 1289–1295. [CrossRef]
141. Maund, J.R.; Smartt, S.J. Hubble Space Telescope imaging of the progenitor sites of six nearby core-collapse supernovae. *Mon. Not. R. Astron. Soc.* **2005**, *360*, 288–304. [CrossRef]
142. Kilpatrick, C.D.; Izzo, L.; Bentley, R.O.; Chambers, K.C.; Coulter, D.A.; Drout, M.R.; de Boer, T.; Foley, R.J.; Gall, C.; Halford, M.R.; et al. Type II-P supernova progenitor star initial masses and SN 2020jfo: Direct detection, light-curve properties, nebular spectroscopy, and local environment. *Mon. Not. R. Astron. Soc.* **2023**, *524*, 2161–2185. [CrossRef]
143. Van Dyk, S.D. The direct identification of core-collapse supernova progenitors. *Philos. Trans. R. Soc. Lond. Ser. A* **2017**, *375*, 20160277. [CrossRef] [PubMed]
144. Dessart, L.; Livne, E.; Waldman, R. Determining the main-sequence mass of Type II supernova progenitors. *Mon. Not. R. Astron. Soc.* **2010**, *408*, 827–840. [CrossRef]
145. Anderson, J.P.; Dessart, L.; Gutiérrez, C.P.; Krühler, T.; Galbany, L.; Jerkstrand, A.; Smartt, S.J.; Contreras, C.; Morrell, N.; Phillips, M.M.; et al. The lowest-metallicity type II supernova from the highest-mass red supergiant progenitor. *Nat. Astron.* **2018**, *2*, 574–579. [CrossRef]
146. O'Connor, E.; Ott, C.D. Black Hole Formation in Failing Core-Collapse Supernovae. *Astrophys. J.* **2011**, *730*, 70. [CrossRef]
147. O'Connor, E. Neutrino Emission from Core-Collapse Supernovae. In Proceedings of the American Astronomical Society Meeting Abstracts #225, Seattle, WA, USA, 4–8 January 2015; Volume 225, p. 121.05.
148. Müller, B.; Heger, A.; Liptai, D.; Cameron, J.B. A simple approach to the supernova progenitor-explosion connection. *Mon. Not. R. Astron. Soc.* **2016**, *460*, 742–764. [CrossRef]
149. Sukhbold, T.; Ertl, T.; Woosley, S.E.; Brown, J.M.; Janka, H.T. Core-collapse Supernovae from 9 to 120 Solar Masses Based on Neutrino-powered Explosions. *Astrophys. J.* **2016**, *821*, 38. [CrossRef]
150. Schneider, F.R.N.; Podsiadlowski, P.; Laplace, E. Pre-supernova evolution and final fate of stellar mergers and accretors of binary mass transfer. *Astron. Astrophys.* **2024**, *686*, A45. [CrossRef]
151. Kochanek, C.S. On the red supergiant problem. *Mon. Not. R. Astron. Soc.* **2020**, *493*, 4945–4949. [CrossRef]
152. Davies, B.; Beasor, E.R. The 'red supergiant problem': The upper luminosity boundary of Type II supernova progenitors. *Mon. Not. R. Astron. Soc.* **2020**, *493*, 468–476. [CrossRef]

153. Healy, S.; Horiuchi, S.; Ashall, C. The Red Supergiant Problem: As Seen from the Local Group's Red Supergiant Populations. *arXiv* **2024**, arXiv:2412.04386. [CrossRef]
154. Beasor, E.R.; Smith, N.; Jencson, J.E. The Red Supergiant Progenitor Luminosity Problem. *Astrophys. J.* **2025**, *979*, 117. [CrossRef]
155. Gal-Yam, A. Observational and Physical Classification of Supernovae. In *Handbook of Supernovae*; Alsabti, A.W., Murdin, P., Eds.; Springer: Cham, Switzerland, 2017; p. 195. [CrossRef]
156. Shivvers, I.; Modjaz, M.; Zheng, W.; Liu, Y.; Filippenko, A.V.; Silverman, J.M.; Matheson, T.; Pastorello, A.; Graur, O.; Foley, R.J.; et al. Revisiting the Lick Observatory Supernova Search Volume-limited Sample: Updated Classifications and Revised Stripped-envelope Supernova Fractions. *Publ. Astron. Soc. Pac.* **2017**, *129*, 054201. [CrossRef]
157. Graur, O.; Bianco, F.B.; Huang, S.; Modjaz, M.; Shivvers, I.; Filippenko, A.V.; Li, W.; Eldridge, J.J. LOSS Revisited. I. Unraveling Correlations Between Supernova Rates and Galaxy Properties, as Measured in a Reanalysis of the Lick Observatory Supernova Search. *Astrophys. J.* **2017**, *837*, 120. [CrossRef]
158. Yoon, S.C. Evolutionary Models for Type Ib/c Supernova Progenitors. *Publ. Astron. Soc. Aust.* **2015**, *32*, e015. [CrossRef]
159. Eldridge, J.J.; Fraser, M.; Smartt, S.J.; Maund, J.R.; Crockett, R.M. The death of massive stars—II. Observational constraints on the progenitors of Type Ibc supernovae. *Mon. Not. R. Astron. Soc.* **2013**, *436*, 774–795. [CrossRef]
160. Van Dyk, S. *A Wolf-Rayet Progenitor for iPTF13bvn*? European Space Agency: Paris, France, 2014.
161. Woosley, S.E.; Bloom, J.S. The Supernova Gamma-Ray Burst Connection. *Annu. Rev. Astron. Astrophys.* **2006**, *44*, 507–556. [CrossRef]
162. Gangopadhyay, A.; Misra, K.; Pastorello, A.; Sahu, D.K.; Tomasella, L.; Tartaglia, L.; Singh, M.; Dastidar, R.; Srivastav, S.; Ochner, P.; et al. SN 2015as: A low-luminosity Type IIb supernova without an early light-curve peak. *Mon. Not. R. Astron. Soc.* **2018**, *476*, 3611–3630. [CrossRef]
163. Gangopadhyay, A.; Misra, K.; Sahu, D.K.; Wang, S.Q.; Kumar, B.; Li, L.; Anupama, G.C.; Dastidar, R.; Elias-Rosa, N.; Kumar, B.; et al. Optical studies of two stripped-envelope supernovae—SN 2015ap (Type Ib) and SN 2016P (Type Ic). *Mon. Not. R. Astron. Soc.* **2020**, *497*, 3770–3789. [CrossRef]
164. Gangopadhyay, A.; Maeda, K.; Singh, A.; Nayana, A.J.; Nakaoka, T.; Kawabata, K.S.; Taguchi, K.; Singh, M.; Chandra, P.; Ryder, S.D.; et al. Bridging between Type IIb and Ib Supernovae: SN IIb 2022crv with a Very Thin Hydrogen Envelope. *Astrophys. J.* **2023**, *957*, 100. [CrossRef]
165. Singh, M.; Misra, K.; Sahu, D.K.; Dastidar, R.; Gangopadhyay, A.; Srivastav, S.; Anupama, G.C.; Bose, S.; Lipunov, V.; Chakradhari, N.K.; et al. Observational properties of a Type Ib supernova MASTER OT J120451.50+265946.6 in NGC 4080. *Mon. Not. R. Astron. Soc.* **2019**, *485*, 5438–5452. [CrossRef]
166. Drout, M.R.; Soderberg, A.M.; Gal-Yam, A.; Cenko, S.B.; Fox, D.B.; Leonard, D.C.; Sand, D.J.; Moon, D.S.; Arcavi, I.; Green, Y. The First Systematic Study of Type Ibc Supernova Multi-band Light Curves. *Astrophys. J.* **2011**, *741*, 97. [CrossRef]
167. Modjaz, M.; Blondin, S.; Kirshner, R.P.; Matheson, T.; Berlind, P.; Bianco, F.B.; Calkins, M.L.; Challis, P.; Garnavich, P.; Hicken, M.; et al. Optical Spectra of 73 Stripped-envelope Core-collapse Supernovae. *Astron. J.* **2014**, *147*, 99. [CrossRef]
168. Liu, Y.Q.; Modjaz, M.; Bianco, F.B.; Graur, O. Analyzing the Largest Spectroscopic Data Set of Stripped Supernovae to Improve Their Identifications and Constrain Their Progenitors. *Astrophys. J.* **2016**, *827*, 90. [CrossRef]
169. Prentice, S.J.; Mazzali, P.A.; Pian, E.; Gal-Yam, A.; Kulkarni, S.R.; Rubin, A.; Corsi, A.; Fremling, C.; Sollerman, J.; Yaron, O.; et al. The bolometric light curves and physical parameters of stripped-envelope supernovae. *Mon. Not. R. Astron. Soc.* **2016**, *458*, 2973–3002. [CrossRef]
170. Sanders, N.E.; Soderberg, A.M.; Levesque, E.M.; Foley, R.J.; Chornock, R.; Milisavljevic, D.; Margutti, R.; Berger, E.; Drout, M.R.; Czekala, I.; et al. A Spectroscopic Study of Type Ibc Supernova Host Galaxies from Untargeted Surveys. *Astrophys. J.* **2012**, *758*, 132. [CrossRef]
171. Schlegel, E.M. A new subclass of type II supernovae ? *Mon. Not. R. Astron. Soc.* **1990**, *244*, 269–271.
172. Schulze, S.; Gal-Yam, A.; Dessart, L.; Miller, A.A.; Woosley, S.E.; Yang, Y.; Bulla, M.; Yaron, O.; Sollerman, J.; Filippenko, A.V.; et al. Extremely stripped supernova reveals a silicon and sulfur formation site. *Nature* **2025**, *644*, 634–639. [CrossRef]
173. Gal-Yam, A.; Yaron, O.; Schulze, S. Introducing a new supernova classification type: SN Ien. *Transient Name Serv. Astronote* **2024**, *239*, 1.
174. Perley, D.A.; Fremling, C.; Sollerman, J.; Miller, A.A.; Dahiwale, A.S.; Sharma, Y.; Bellm, E.C.; Biswas, R.; Brink, T.G.; Bruch, R.J.; et al. The Zwicky Transient Facility Bright Transient Survey. II. A Public Statistical Sample for Exploring Supernova Demographics. *Astrophys. J.* **2020**, *904*, 35. [CrossRef]
175. Hosseinzadeh, G.; Arcavi, I.; Valenti, S.; McCully, C.; Howell, D.A.; Johansson, J.; Sollerman, J.; Pastorello, A.; Benetti, S.; Cao, Y.; et al. Type Ibn Supernovae Show Photometric Homogeneity and Spectral Diversity at Maximum Light. *Astrophys. J.* **2017**, *836*, 158. [CrossRef]
176. Pellegrino, C.; Howell, D.A.; Terreran, G.; Arcavi, I.; Bostroem, K.A.; Brown, P.J.; Burke, J.; Dong, Y.; Gilkis, A.; Hiramatsu, D.; et al. The Diverse Properties of Type Icn Supernovae Point to Multiple Progenitor Channels. *Astrophys. J.* **2022**, *938*, 73. [CrossRef]

177. Fullerton, A.W.; Massa, D.L.; Prinja, R.K. The Discordance of Mass-Loss Estimates for Galactic O-Type Stars. *Astrophys. J.* **2006**, *637*, 1025–1039. [CrossRef]
178. Sana, H.; de Mink, S.E.; de Koter, A.; Langer, N.; Evans, C.J.; Gieles, M.; Gosset, E.; Izzard, R.G.; Le Bouquin, J.B.; Schneider, F.R.N. Binary Interaction Dominates the Evolution of Massive Stars. *Science* **2012**, *337*, 444. [CrossRef]
179. Smith, N.; Li, W.; Foley, R.J.; Wheeler, J.C.; Pooley, D.; Chornock, R.; Filippenko, A.V.; Silverman, J.M.; Quimby, R.; Bloom, J.S.; et al. SN 2006gy: Discovery of the Most Luminous Supernova Ever Recorded, Powered by the Death of an Extremely Massive Star like $\eta$ Carinae. *Astrophys. J.* **2007**, *666*, 1116–1128. [CrossRef]
180. Jencson, J.E.; Prieto, J.L.; Kochanek, C.S.; Shappee, B.J.; Stanek, K.Z.; Pogge, R.W. Optical observations of the luminous Type IIn Supernova 2010jl for over 900 d. *Mon. Not. R. Astron. Soc.* **2016**, *456*, 2622–2635. [CrossRef]
181. Gangopadhyay, A.; Turatto, M.; Benetti, S.; Misra, K.; Kumar, B.; Cappellaro, E.; Pastorello, A.; Tomasella, L.; Vanni, S.; Fiore, A.; et al. Photometric and spectroscopic evolution of the peculiar Type IIn SN 2012ab. *Mon. Not. R. Astron. Soc.* **2020**, *499*, 129–148. [CrossRef]
182. Pastorello, A.; Cappellaro, E.; Inserra, C.; Smartt, S.J.; Pignata, G.; Benetti, S.; Valenti, S.; Fraser, M.; Takáts, K.; Benitez, S.; et al. Interacting Supernovae and Supernova Impostors: SN 2009ip, is this the End? *Astrophys. J.* **2013**, *767*, 1. [CrossRef]
183. Gangopadhyay, A.; Dukiya, N.; Moriya, T.J.; Tanaka, M.; Maeda, K.; Howell, D.A.; Singh, M.; Singh, A.; Sollerman, J.; Kawabata, K.S.; et al. SN 2021foa: The bridge between SN IIn and Ibn. *Mon. Not. R. Astron. Soc.* **2025**, *537*, 2898–2917. [CrossRef]
184. Goto, S.; Yamanaka, M.; Nagayama, T.; Maeda, K.; Kawabata, M.; Sahu, D.K.; Singh, A.; Gangopadhyay, A.; Dkuniya, N.; Misra, K.; et al. SN 2023vbg: A Type IIn Supernova Resembling SN 2009ip, with a Long-Duration Precursor and Early-Time Bump. *arXiv* **2025**, arXiv:2504.15988. [CrossRef]
185. Chugai, N.N. Broad emission lines from the opaque electron-scattering environment of SN 1998S. *Mon. Not. R. Astron. Soc.* **2001**, *326*, 1448–1454. [CrossRef]
186. Smith, N.; Chornock, R.; Li, W.; Ganeshalingam, M.; Silverman, J.M.; Foley, R.J.; Filippenko, A.V.; Barth, A.J. SN 2006tf: Precursor Eruptions and the Optically Thick Regime of Extremely Luminous Type IIn Supernovae. *Astrophys. J.* **2008**, *686*, 467–484. [CrossRef]
187. Brennan, S.J.; Schulze, S.; Lunnan, R.; Sollerman, J.; Yan, L.; Fransson, C.; Irani, I.; Melinder, J.; Chen, T.W.; De, K.; et al. SN 2021adxl: A luminous nearby interacting supernova in an extremely low-metallicity environment. *Astron. Astrophys.* **2024**, *690*, A259. [CrossRef]
188. Bilinski, C.; Smith, N.; Williams, G.G.; Smith, P.S.; Leonard, D.C.; Hoffman, J.L.; Andrews, J.E.; Milne, P. Multi-epoch spectropolarimetry for a sample of Type IIn Supernovae: Persistent asymmetry in dusty circumstellar material. *Mon. Not. R. Astron. Soc.* **2024**, *529*, 1104–1129. [CrossRef]
189. Gangopadhyay, A.; Misra, K.; Hosseinzadeh, G.; Arcavi, I.; Pellegrino, C.; Wang, X.; Andrew Howell, D.; Burke, J.; Zhang, J.; Kawabata, K.; et al. Evolution of a Peculiar Type Ibn Supernova SN 2019wep. *Astrophys. J.* **2022**, *930*, 127. [CrossRef]
190. Gangopadhyay, A.; Sollerman, J.; Tsalapatas, K.; Maeda, K.; Dukiya, N.; Schulze, S.; Fransson, C.; Sarin, N.; Pessi, P.J.; Singh, M.; et al. SN 2023xgo: Helium-rich Type Icn or Carbon-Flash Type Ibn supernova? *Mon. Not. R. Astron. Soc.* **2025**. [CrossRef]
191. Hiramatsu, D.; Berger, E.; Gomez, S.; Blanchard, P.K.; Kumar, H.; Athukoralalage, W. Type IIn Supernovae. I. Uniform Light Curve Characterization and a Bimodality in the Radiated Energy Distribution. *arXiv* **2024**, arXiv:2411.07287. [CrossRef]
192. Dastidar, R.; Pignata, G.; Dukiya, N.; Misra, K.; Hiramatsu, D.; Silva-Farfán, J.; Andrew Howell, D.; Azalee Bostroem, K.; Singh, M.; Gangopadhyay, A.; et al. SN 2019nyk: A rapidly declining Type II supernova with early interaction signatures. *Astron. Astrophys.* **2024**, *685*, A44. [CrossRef]
193. Ivezić, Ž.; Kahn, S.M.; Tyson, J.A.; Abel, B.; Acosta, E.; Allsman, R.; Alonso, D.; AlSayyad, Y.; Anderson, S.F.; Andrew, J.; et al. LSST: From Science Drivers to Reference Design and Anticipated Data Products. *Astrophys. J.* **2019**, *873*, 111. [CrossRef]
194. Lochner, M.; Scolnic, D.M.; Awan, H.; Regnault, N.; Gris, P.; Mandelbaum, R.; Gawiser, E.; Almoubayyed, H.; Setzer, C.N.; Huber, S.; et al. Optimizing the LSST Observing Strategy for Dark Energy Science: DESC Recommendations for the Wide-Fast-Deep Survey. *arXiv* **2018**, arXiv:1812.00515. [CrossRef]
195. Gris, P.; Regnault, N.; Awan, H.; Hook, I.; Jha, S.W.; Lochner, M.; Sanchez, B.; Scolnic, D.; Sullivan, M.; Yoachim, P.; et al. Designing an Optimal LSST Deep Drilling Program for Cosmology with Type Ia Supernovae. *Astrophys. J.* **2023**, *264*, 22. [CrossRef]
196. Mitra, A.; Gómez-Vargas, I.; Zarikas, V. Dark energy reconstruction analysis with artificial neural networks: Application on simulated Supernova Ia data from Rubin Observatory. *Phys. Dark Universe* **2024**, *46*, 101706. [CrossRef]
197. Petrecca, V.; Botticella, M.T.; Cappellaro, E.; Greggio, L.; Sánchez, B.O.; Möller, A.; Sako, M.; Graham, M.L.; Paolillo, M.; Bianco, F.; et al. Recovered supernova Ia rate from simulated LSST images. *Astron. Astrophys.* **2024**, *686*, A11. [CrossRef]
198. Jacobson-Galán, W.V.; Dessart, L.; Jones, D.O.; Margutti, R.; Coppejans, D.L.; Dimitriadis, G.; Foley, R.J.; Kilpatrick, C.D.; Matthews, D.J.; Rest, S.; et al. Final Moments. I. Precursor Emission, Envelope Inflation, and Enhanced Mass Loss Preceding the Luminous Type II Supernova 2020tlf. *Astrophys. J.* **2022**, *924*, 15. [CrossRef]
199. Fuller, J. Pre-supernova outbursts via wave heating in massive stars—I. Red supergiants. *Mon. Not. R. Astron. Soc.* **2017**, *470*, 1642–1656. [CrossRef]

200. Nugent, P.E.; Sullivan, M.; Cenko, S.B.; Thomas, R.C.; Kasen, D.; Howell, D.A.; Bersier, D.; Bloom, J.S.; Kulkarni, S.R.; Kandrashoff, M.T.; et al. Supernova SN 2011fe from an exploding carbon-oxygen white dwarf star. *Nature* **2011**, *480*, 344–347. [CrossRef]
201. Yaron, O.; Prialnik, D.; Kovetz, A.; Shara, M.M. An Extensive Grid of Models Producing Extreme Horizontal Branch Stars. *arXiv* **2017**, arXiv:1709.02127. [CrossRef]